# POLITECNICO DI MILANO

**Scuola di Ingegneria Industriale e dell'Informazione**


**Master of Science in Automation and Control Engineering**

# ROBUST HARMONIC CONTROL
# AN APPLICATION TO STRUCTURAL VIBRATION REDUCTION IN HELICOPTERS

*Supervisor:*
Prof. Marco Lovera

Master Thesis by:
Ho Duc Du
Student Id: 800867

Academic Year 2013/2014

# POLITECNICO DI MILANO

**Scuola di Ingegneria Industriale e dell'Informazione**


**Master of Science in Automation and Control Engineering**

# ROBUST HARMONIC CONTROL
# AN APPLICATION TO STRUCTURAL VIBRATION REDUCTION IN HELICOPTERS

*Supervisor:*
Prof. Marco Lovera

Master Thesis by:
Ho Duc Du
Student Id: 800867

Academic Year 2013/2014

*"Learn from yesterday, live for today, hope for tomorrow. The important thing is not to stop questioning.."*

Albert Einstein

# Abstract

In this thesis, the problem in designing the robust multivariable controllers for the reduction of the vibration response in a helicopter was addressed. The mathematical model is identified from data collected on an A109 Agusta helicopter, in which a set of piezoelectric actuators and accelerometers are mounted on its fuselage. The interactions in plant model are then handled through two pre-compensators which are relied on the Relative Gain Array. The active harmonic control approach is proposed to guarantee performance in the closed-loop system.

In detail, the model was analyzed firstly to select the input-output pairings though two approaches such as Singular Value Decomposition and Relative Gain Array. These results showed that an output of MIMO system is influenced significantly by two actuators as compared with the rest. However, to further simplify the tuning of the controllers, a compensator design approach for the decoupling of the plant model, based on Relative Gain Array was proposed.

Afterwards, the LQR and $H_\infty$ control synthesis techniques were implemented, based on the compensated model. While the former is able to deal with only the nominal identified model, the latter takes model uncertainties into account, which are supposed to be output uncertainties. To compare the performance levels achieved by two design approaches, the MonteCarlo simulation has been carried out, by randomly perturbing 500 times of $T$-matrix based on its uncertainty representation.

**Keywords**: control structure design, relative gain array, non square model, LQR, $H_\infty$.

# Acknowlegements

A lot of people have helped me during the work of this thesis. First of all, I would like to thank my supervisor Prof. Marco Lovera for guiding me in this thesis and spending time in discussion to answer my questions. I also am grateful to Roberto Mura who helped me in designing the controllers and giving me the useful advices.

Finally, I want to thank my friend Thanh Tra Nguyen for her grammar corrections and mental supports, my family for their unconditioned love.

# Contents

# List of Figures

# List of Tables

# Abbreviations

| | |
|---|---|
| **UAV** | Unnamed Autonomous Vehicle |
| **MIMO** | Multi Inputs Multi Outputs |
| **SISO** | Single Input Single Output |
| **SVD** | Singular Value Decomposition |
| **RGA** | Relative Gain Array |
| **HHC** | Higher Harmonic Control |
| **IBC** | Individual Blade Control |
| **ACSR** | Active Control of Structural Response |
| **ATR** | Active Twist Rotor Blades |
| **ACF** | Actively Controlled Flaps |
| **LQ** | Linear Quadratic |

*To my family*

# Chapter 1

# Introduction

## 1.1 Introduction

The helicopter has become an important mode of aerial transportation primarily due to its unique ability not only in taking-off and landing vertically but also in hovering. These properties of helicopters enable many unique tasks such as rescue operation in civilian, firefighting operation in mountains and military application. In general, the use of helicopters has increased in the last few decades, especially in civilian applications, and is expected to continue in the future. However, high vibration levels have effected poorly to the passengers and crew (also because of the acoustic noise they generate), besides causing various undesirable effects, such as degradation of the structural integrity, increase in the fatigue of the mechanical components, and reduction of the effectiveness of the on-board computer systems. In the satisfaction of pilots point of view, undesired vibrations transmitted to fuselage have been known to cause fatigue and discomfort to the aircrew and passengers in the short-term as well as the back pain injuries due to the long term. For example, the sound pressure level of noise measured in the helicopter cabin is on average from 20 to 30 dB higher than those of fixed wing aircraft [2]. In particular, the acoustic components' frequencies are typically varied from 500Hz to 4500Hz to which the human ear is the most sensitive. Moreover, in the case of unmanned vehicles, which are frequently employed to carry out data and image acquisition tasks using sensitive equipment, vibrations can lead to a non negligible degradation of the mission characteristics [3], so that studies aimed at improving UAV performance in this respect are ongoing, both in the rotary wing and in the fixed wing literature [4].

On the other hand, on helicopters, vibrations originate from the main rotor, the tail rotor, the engines and other machinery [5]. In particular, the main gearbox, which powers the main and tail rotors, is rigidly mounted on the roof structure of the helicopter

via connecting elements called struts through which vibrations are transmitted to the cabin roof. While the frequencies of the disturbance created by the main rotor are integer multiples of the rotor angular frequency, vibrations induced by the gearbox have a much wider spectrum which is related to the angular rates of the individual reduction stages.

## 1.2 Problem Statement

Active vibration reduction techniques which are illustrated schematically in Figure 1.1 have been introduced to overcome the limitations imposed by passive control techniques and to increase the attenuation of both noise and vibrations [6]. An active control system consists of four main components: a set of sensors, a set of actuators, a power supply unit and a controller. The acoustic noise signals or vibrations are measured by sensors mounted on the fuselage. The signals are then processed by the controller and used to generate a signal to drive the actuators. The actuators are controlled to produce a vibration field that compensates as closely as possible the unwanted vibrations.

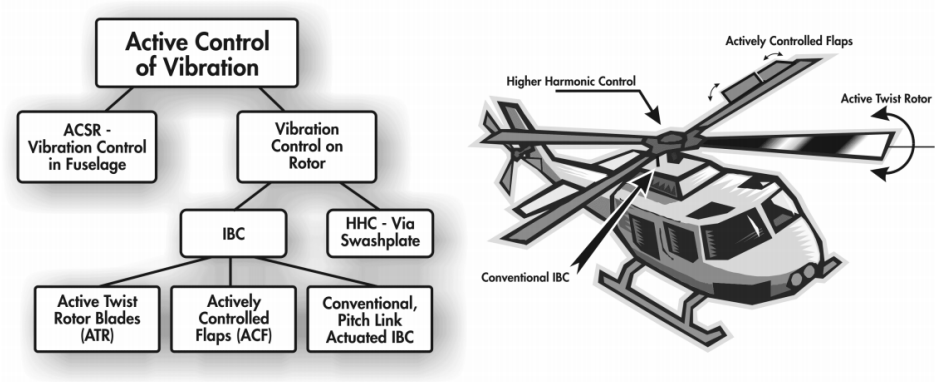


FIGURE 1.1: *An overview of active vibration reduction techniques.*

The HHC and IBC methods aim at reducing the noise before it propagate to the fuselage by means of actuators placed on the rotor while the ACSR attenuates only the noise in the fuselage. However, the ACSR depicted in Figure 1.2 is currently one of the most popular helicopter vibration attenuation methods. A set of sensors are mounted at key positions in the fuselage, where the minimum noise is desired (for example at passenger seat). An ACSR controller uses the sensors' signals to manipulate the behaviors of actuators in order to reduce the vibrations. This technology has been applied in modern helicopters such as the Augusta/Westland AW101.

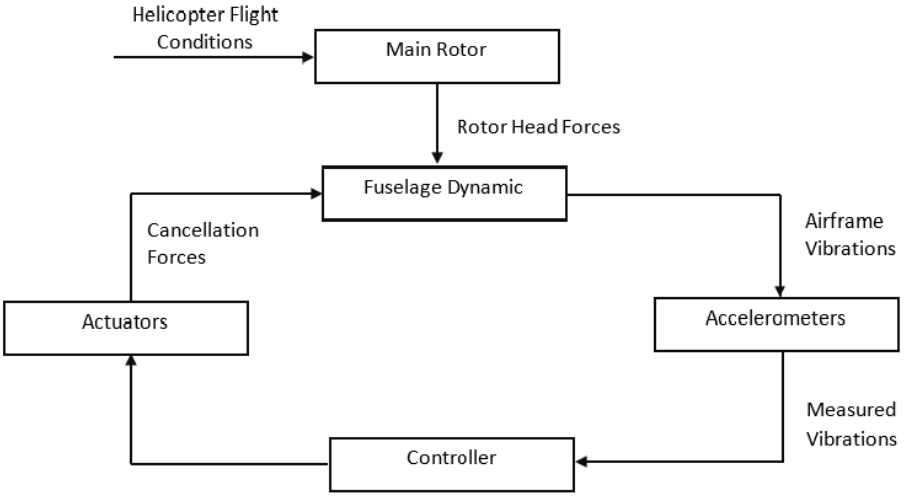


FIGURE 1.2: *Scheme of ACSR vibration attenuation system.*

The problem of designing control laws for this application can be formulated either in a model-based or in a model-free way. Regardless of this choice, however, the availability of a representative mathematical model of the response of the system to excitation applied to the actuators is a prerequisite for the possibility of developing control laws in simulation and assessing their performance prior to actual implementation on the real system. Furthermore, in view of the strongly multi-variable nature of the problem the ability to exploit a reliable model to structure the control system is an extremely valuable asset. Unfortunately working out a qualitatively accurate model of structural response from first principles is not feasible, so an experimental approach must be envisaged.

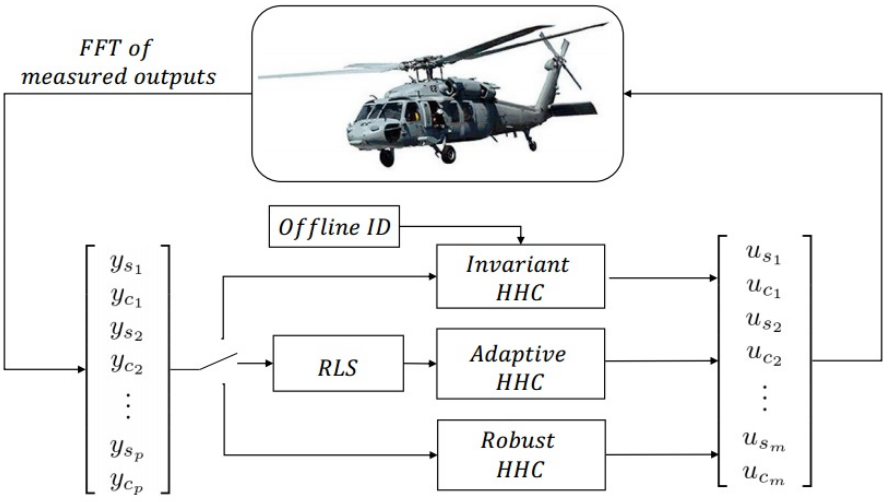


FIGURE 1.3: *An overview of HHC for active vibration reduction techniques.*

In the view of above discussion, the MIMO models have been sought in order to address with the problem of modeling the structural response and then the Harmonic Control (HC) which is depicted in the Figure 1.3 has been applied for the design and implementation of control laws [7].

## 1.3 Literature review

From the identification point of view, the experimental results presented in this thesis have been obtained on the facility available at the Department of Aerospace Science and Technology of the Politecnico di Milano, described in detail in the following section, which was set up in the framework of the *Friendcopter* project [8]. The model identification problem is particularly involved in view of the large size of the system (40 inputs and 18 outputs), which makes it difficult to achieve adequate accuracy on all channels. An expected outcome of the identification analysis is an indication on how to simplify the multivariable structure of the system in view of the control design. The identification was carried out with different techniques to obtain satisfactory results. Since the control objective is the attenuation at specific frequencies the use of suitable data prefiltering has been investigated to achieve more accuracy at the selected frequencies.

In the control design point of view, Harmonic Control (HC) has been considered for many years as a valid approach for the design and implementation of control laws aimed at vibration attenuation in helicopters. Its basic idea is to attenuate the vibratory components in the fuselage accelerations by adding suitably phased harmonic components to the controls. Several studies have been carried out to determine the feasibility of HC both from the theoretical and the experimental viewpoint [9] [10, 11] where the used actuation technologies, the considered performance criteria (*e.g.,* noise, vibrations, power, loads etc.) and the achieved performance are reviewed. As for the control implementation, a discrete-time adaptive algorithm known in the rotorcraft literature as the $T - matrix$ algorithm [12]( where this approach was originally proposed) is typically used by defining the problem in the frequency domain and tuning the controller using an LQ-like cost function. In this thesis the robust design approach for HC control laws proposed in [13] [14] is applied to the problem of structural vibration attenuation. The approach provides nominal stability of the closed-loop system, robustness to model uncertainty and guaranteed performance for the closed-loop system, i.e., a guaranteed level of vibration attenuation. The $H_\infty$ formulation of the HC problem provides an additional benefit when dealing with the tuning problem. Indeed, vibrations are typically measured on the fuselage in a large number of locations, so the control problem

is strongly multivariables, with different performance requirements associated to the vibration attenuation on the individual outputs. Requirement specifications in terms of steady state attenuation levels and desired transient performance can be immediately "encoded" in an $H_\infty$ problem statement and the properties of the optimal solution can provide information about the actual distance between the desired and the achievable performance level. To further simplify the tuning of the controller, a novel approach to the decoupling of the plant model, based on the Relative Gain Array (RGA) [1] is proposed in order to compare with the result obatined for non-square chemical plant [15].

## 1.4 Contribution of the thesis

The main contributions of this thesis are:

- Selection the suitable pairings among the set of inputs and outputs by singular value decomposition and relative gain array.
- Develop compensator based on relative gain array properties for non-square model.
- Design of LQR and robust controllers for each sub-compensated-plant.

## 1.5 Thesis outline

This section provides a brief overview of the organization of this work.

- Chapter 1 summarizes the most important aspects about active vibration attenuation in helicopter.
- Chapter 2, on the other hand, illustrates the experimental set-up for test bench in *Friendcopter* project and gives the short instruction how to select the test signal for this identification.
- Chapter 3 presents the motivation for this research and a brief background on need for helicopter vibration attenuation control. It included the significance of the thesis, objectives and the main contributions which are given in the present chapter.
- Chapter 4 presents the basic background and theoretical properties. Specifically, it describes the characteristic of relative gain array, whose are using in finding suitable compensator in case of non-square model.

- In chapter 5, the LQR and $H_\infty$ synthesis methods are described. The design of both controllers has been based on the compensated model which has been obtained.
- Chapter 6 presents the simulation results and discusses in detail about the advantages and drawbacks of the procedure.
- Finally, chapter 7 concludes by summarizing the results of this research effort and recommends the development for future work.

# Chapter 2

# The experimental set-up

In this chapter, the description of the experimental facility used in the framework of the *Friendcopter* project will be proposed. The model identification problem is particularly involved in view of the large dimensions of the input and output vectors of the system (40 inputs and 18 outputs ), which makes it difficult to achieve adequate accuracy on all channels. An expected outcome of the identification analysis is an indication on how to simply the multivariable structure of the system in control design point of view.

Hence, the chapter is structured as follows:

- **Description of experimental set-up:** The experiment model is introduced for identifying the frequency response between actuators and accelerometers.
- **Decision of type and position of actuators and accelerometers:** The choices of actuators, accelerometers and their locations in the Agusta A109 MKII helicopter are proposed.
- **Disturbance frequencies:** The choice of disturbance frequencies in the experiment is made.
- **Acquisition system:** This section describes the hardware and software use in experiment in order to acquire the signals.
- **Problem statement:** The objective of the work which will be solved in the next chapters is introduced.
- **Conclusion:** This subsection concludes the chapter.

## 2.1 Description of the experimental set-up

The employed set-up, illustrated in Figure 2.1, is an actual fuselage of an Agusta A109 MKII helicopter, without blades, tail rotor, pumps, internal equipment, but equipped with the main components of the rotor and structural links. To simulate in-flight conditions an aerodynamic brake (shown in Figure 2.2) was mounted; the main gearbox is powered by two electric motors which drive it in place of the helicopter turbines. Even


FIGURE 2.1: Helicopter fuselage mock-up employed in the *Friendcopter* project.

FIGURE 2.2: Aerodynamic brake.

though the set-up lacks some of the noise-generating devices (such as, pumps and tail rotor), the current configuration allows to reproduce the disturbance tones generated by the main rotor gearbox [8]. Indeed, the gearbox is connected to the fuselage with a set of rigid struts and an aluminum anti-torque plate mounted above the cabin roof. In this

way, all the loads generated by the rotor are transmitted to the anti-torque plate instead of the struts. A typical shape of the anti-torque plate is shown in Figure 2.3. The generated vibrations are transmitted to the fuselage mainly through the anti-torque plate and the rear struts, so in view of developing an active system for vibration reduction, actuators have been mounted on these components..

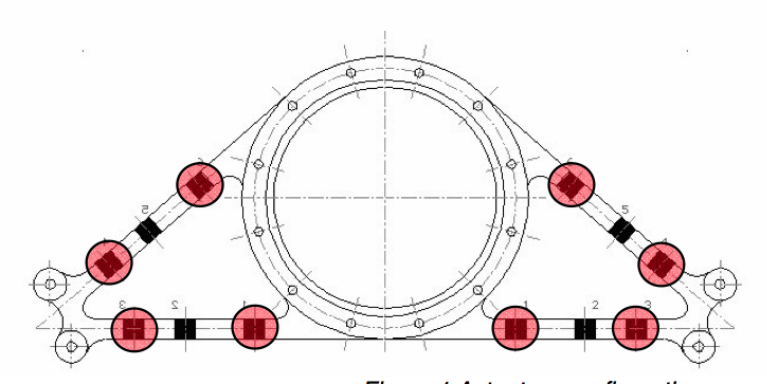

FIGURE 2.3: Anti-torque plate.

## 2.2 Decision of type and position of actuators and accelerometers

Piezoelectric patches are suitable actuators for this application, considering that they are not bulky and do not significantly affect the mechanical structure. Sixteen patches were placed on the two rear struts (8 on the left one and 8 on the right one) and 24 on the anti-torque plate (12 on the left side and 12 on the right side) for a total of 40 actuators. No actuator was placed on the front struts because no significant vibration field was detected in the part of the roof corresponding to their structural attachments to the cabin. The actuators location is shown in Figure 2.4.

As far as sensors are concerned, accelerometers have been used. More specifically, 18 accelerometers have been placed on the cabin roof (9 per side), in correspondence to the points of structural attachment of the anti-torque plate and the rear struts, as well as in other locations characterized by high vibration levels (see Figure 2.5).

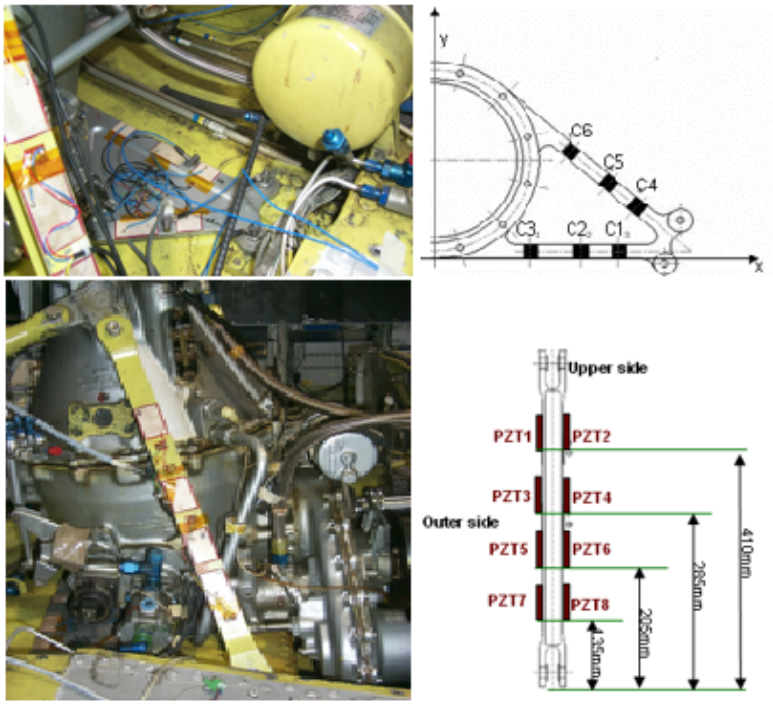


FIGURE 2.4: Anti-torque plate.


FIGURE 2.5: Location of the accelerometers.

## 2.3 Disturbance frequencies

In order to achieve high fidelity models, the most crucial step in system identification is collecting appropriate informative data. The informative data is usually obtained by either applying mining algorithms to historical data or performing a system identification

experiment. For the vibratory test bench, it was decided to perform an identification experiment. The choice of input test signals is generally the most important consideration in system identification. Hence, in order to assess the ability of the test bench to replicate the vibratory phenomena typical of in-flight conditions, a comparison between vibration spectra collected on the test facility and corresponding spectra measured in flight was carried out. The result of the comparison is shown in Figure 2.6, from which it is apparent that the qualitative agreement is satisfactory, even though, as already mentioned, the test bench is not entirely representative from the quantitative point of view, as a number of significant sources of excitation is missing.

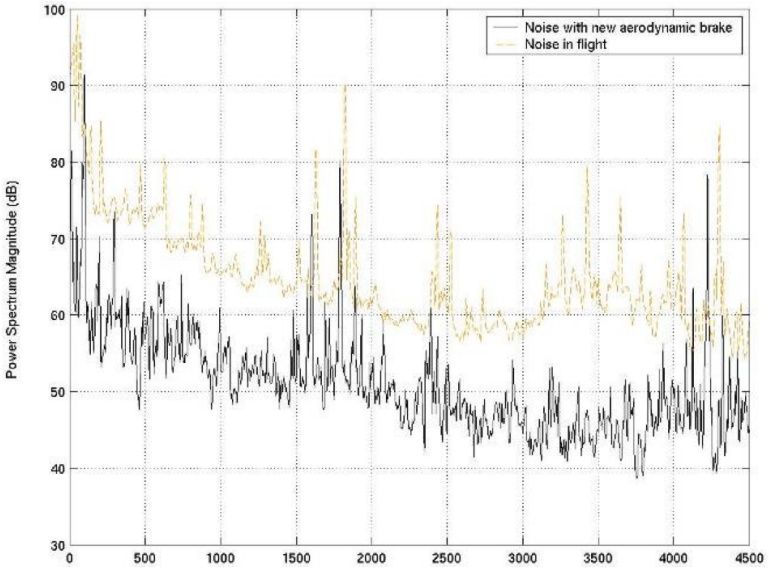


FIGURE 2.6: Noise spectrum inside the cabin.

The spectra reported in Figure 2.6 also provide some insight in the disturbances which the control system is called to counteract. Indeed, besides the large low frequency components ($< 200$ Hz), there are several significant peaks in the speech frequency range, that are especially annoying from an acoustic point of view (in the case of manned vehicles), namely at frequencies 1599 Hz, 1785 Hz, 2400 Hz, and 4250 Hz. The attenuation of these high frequency tones is the main objective of the ongoing study.

## 2.4 Acquisition system

The acquisition system employed in the project consists of two PCI's (PCI-6251, PCI-MIO-16E-1) that are used to acquire the accelerometric signals and to generate the excitation signals for the actuators. The generated signals are low-pass filtered (cut-off at 5 kHz) and amplified by a factor of 20. The accelerometers are connected to

the 478A16 signal conditioners that provide the voltage supply needed by the sensors. The software used to set the devices and to perform the experiments is NI LabVIEW SignalExpress. The sampling frequency was set to 10 kHz and the cut-off frequency of the anti-aliasing and reconstruction filters was set to 5 kHz. KEMO 8 BenchMaster 21M filters have been employed. All subsequent data processing has been carried out using MATLAB.

## 2.5 Problem statement

The goal of this work is to attenuate the acoustic noise and vibrations at least in a specific frequency and reduced volume of the helicopter fuselage. In particular, it is desirable to reduce the noise in the volume where the passengers are supposed to sit. This is typically achieved with active techniques as the ones which will be described in the next chapters. On the other hand, the reliable model of the system is a combination of the large number of inputs and outputs that makes the controller design process more difficult. Hence, new techniques are developed based on the RGA and SVD to obtain the decentralized system in which a control algorithm for active vibration reduction in helicopters has been synthesized and simulated in order to understand if such a control can be applied to the system.

## 2.6 Conclusion

In conclusion, the helicopter test bench has been installed for noise and vibration control. The identified model is described in detail in [7]. In next chapter, this model will be used to design the controller based on LQ-like and $H_\infty$ techniques.

# Chapter 3

# $T-$Matrix model

In this chapter, the basic notions about single frequency response, T matrix and MIMO non-square model will be introduced. Then the uncertainty representation is discussed. All of the analysis is based on the characteristic of the model. Hence, the chapter is structured as follows:

- **Single frequency $G(s) \rightarrow G(j\omega)$:** This section presents the equivalent representation of transfer function $G(s)$ in Laplace domain and $G(j\omega)$ in frequency domain.
- **T-matrix algorithm:** The algorithm used to separate the sin and cosin elements of the signals in frequency domain are formulated.
- **MIMO non-square plant:** The non-square MIMO model and its properties are presented.
- **Uncertainty representation:** The uncertainty presentation is introduced in order to describe in detail about the output uncertainty model.
- **Conclusion:** This section concludes the chapter.

## 3.1 Single frequency $G(s) \rightarrow G(j\omega)$

In Laplace domain, the transfer function $G(s)$ denotes the relation from inputs to the outputs, which therefore represents the dynamics of the system. Nevertheless, if the Laplace variable $s$ is fixed as equal as $s_0$, then the transfer function $G(s_0)$ is basically an $m \times p$ complex matrix (with $p$ inputs and $m$ outputs),which can be analyzed by using standard matrix algebra tools. More precisely, the choice $s_0 = j\omega$ is of interest because

$G(j\omega)$ represents the frequency response of the system in frequency $\omega$.
Let consider a rational transfer function with input $u(s)$ and output $y(s)$:

$$\frac{y(s)}{u(s)} = G(s) = k\frac{(s+z_1)(s+z_2)\dots}{(s+p_1)(s+p_2)\dots} \tag{3.1}$$

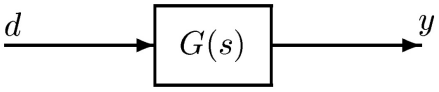


FIGURE 3.1: System G(s) with input $d$ and output $y$. Figure obtained from [1].

which is illustrated in the Figure 3.1. By replacing $s$ with $j\omega$ the above transfer function will become the so-called frequency response model with:

- $g_{ij}$ is the sinusoidal response from input $u_j$ to output $y_i$.

In detail, a sinusoidal input signal of frequency $\omega$ has been applied to the system:

$$u_j = u_{0j}\sin(\omega t + \alpha_j) \tag{3.2}$$

The output of linear system will be another sinusoidal signal with the same frequency as compared as this persistent input signal when $t$ tends to $\infty$.

$$y_i(t) = y_{i0}\sin(\omega t + \beta_i) \tag{3.3}$$

in which, the amplitude and phase of output and input signal are related by the magnitude and phase of the complex number $g_{ij}$ as:

$$\frac{y_{i0}}{u_{j0}} = |g_{ij}(j\omega)|, \qquad \beta_i - \alpha_j = \angle g_{ij}(j\omega) \tag{3.4}$$

As a consequence, the sinusoidal time response described in (3.2)−(3.4) can be represented compactly as follows:

$$y_i(\omega) = g_{ij}(\omega)u_j(\omega) \tag{3.5}$$

where:

$$u_j(\omega) = u_{j0}e^{j\alpha_j}, \qquad y_i(\omega) = y_{i0}e^{j\beta_i} \tag{3.6}$$

Using the super-position principle in linear systems, the overall response to simultaneous input signals with the same frequency in several input channels can be obtained as the

sum of each response from (3.4):

$$y_i(\omega) = g_{i1}(j\omega)u_1(\omega) + g_{i2}(j\omega)u_2(\omega) + \ldots = \sum_j g_{ij}u_j(\omega) \tag{3.7}$$

or in matrix from:

$$y(\omega) = G(j\omega)u(\omega) \tag{3.8}$$

with

$$u(\omega) \begin{bmatrix} u_1(\omega) \\ u_2(\omega) \\ \vdots \\ u_m(\omega) \end{bmatrix} \qquad \text{and} \qquad y(\omega) = \begin{bmatrix} y_1(\omega) \\ y_2(\omega) \\ \vdots \\ y_p(\omega) \end{bmatrix} \tag{3.9}$$

the vectors of sinusoidal input and output signals.

## 3.2 T-matrix algorithm

In the literature, the problem of plant representation in helicopter is traditionally in the frequency domain, using a discrete adaptive algorithm known as $T - Matrix$ algorithm, which is originally proposed by (Shaw and Albion, 1981).
First of all, the definition of T-matrix has implied the relation between the steady state response of aircraft and a proper steady state harmonic input. This means that in order to define the T-matrix for the helicopter, the response of the helicopter model has to be studied with the fixed frequency.
Let define $u \in \mathbb{R}^m$ be a vector of control inputs and $y \in \mathbb{R}^p$ be a vector of harmonic of measured outputs with frequency $\omega$; also assume $u$ to be a piece-wise periodic function of period $T = 2\pi/\omega$, where omega is the disturbance frequency, $\psi = \omega t$, and define

$$y_{Nc}^{(i)} = \frac{2}{T}\int_0^T y^{(i)}(\psi)\cos(N\psi)dt \tag{3.10}$$

$$y_{Ns}^{(i)} = \frac{2}{T}\int_0^T y^{(i)}(\psi)\sin(N\psi)dt \tag{3.11}$$

$$y = \begin{bmatrix} y_{Nc}^{(1)} \\ y_{Ns}^{(1)} \\ \vdots \\ y_{Nc}^{(p)} \\ y_{Ns}^{(p)} \end{bmatrix} \tag{3.12}$$

and similar for $u_N$. Assume now that under steady sate conditions the above defined frequency harmonics of $u_N$ and $y_N$ are related by the linear equation

$$y_N = T_{N,N} u_N + \xi \tag{3.13}$$

in which:

+ $T_{N,N}$ is a $2p \times 2m$ constant coefficient matrix.
+ $\xi$ represent the vibrations effecting to the system in frequency $\omega$.
+ $u_N$ is control input vector which can be similarly defined as:

$$u_N = \begin{bmatrix} \theta_{Nc} \\ \theta_{Ns} \end{bmatrix} \tag{3.14}$$

with $\theta_{Nc}$ and $\theta_{Ns}$ are the cosine and sine components of the control input in frequency $\omega$ respectively.

In this problem, it has to be noticed that the relationship between the input and the outputs can be considered time invariant due to the following reason:

+ The dynamic of rotor is reasonably assumed to be steady, which is not affected by the environment.
+ The actuators and sensors of the higher harmonic systems is located in the fixed positions in the aircraft.

As a consequence, the frequency response matrix $G(j\omega)$ is defined as:

$$G(j\omega) = \begin{bmatrix} G^{(1,1)}(j\omega) & \dots & G^{(1,m)}(j\omega) \\ \vdots & \ddots & \vdots \\ G^{(p,1)}(j\omega) & \dots & G^{(p,m)}(j\omega) \end{bmatrix} \tag{3.15}$$

With $T_{N,N}$ is corresponded with $G(j\omega)$, as

$$T_{N,N} = \begin{bmatrix} Real(G^{(i,j)}(j\omega)) & Imag(G^{(i,j)}(j\omega)) \\ -Imag(G^{(i,j)}(j\omega)) & Real(G^{(i,j)}(j\omega)) \end{bmatrix} \tag{3.16}$$

$T_{N,N}$ therefore is defined as

$$T_{N,N} = \begin{bmatrix} T_{N,N}^{(1,1)} & \dots & T_{N,N}^{(1,m)} \\ \vdots & & \vdots \\ T_{N,N}^{(p,1)} & \dots & T_{N,N}^{(p,m)} \end{bmatrix} \tag{3.17}$$

## 3.3 MIMO non-square plant

Processes with only one output being controlled by a single manipulated variable are classified as single-input single-output (SISO) systems. However, many processes do not comfort to such simple control configuration according to the complex structures and requirements. In the helicopter industries, the common schemes which are used to describe the physical law in the system are Multi inputs multi outputs.

In MIMO, one or more manipulated variables can affect the output variables in a particular loop or all other control loops. A MIMO control structure is crucial in systems that have multiple dependencies and multiple interactions between different variables.

In particular, for the model of the aircraft identified as the non-square model with the number of inputs be higher than outputs. The frequency response matrix is:

$$G(j\omega) = \begin{bmatrix} G^{(1,1)}(j\omega) & \dots & G^{(1,m)}(j\omega) \\ \vdots & \ddots & \vdots \\ G^{(p,1)}(j\omega) & \dots & G^{(p,m)}(j\omega) \end{bmatrix} \tag{3.18}$$

in which, $u \in \mathbb{R}^m$ and $y \in \mathbb{R}^p$ are corresponding to which the size of the model is $p \times m$

## 3.4 Uncertainty representation

The identified model is always imperfect due to the existence of uncertainties. Some of the most original sources of uncertainty are:

- Erroneous in measurement devices.
- Some of the parameters of linear model differ from real parameter due to the estimation, which may even vary with time.
- Although the precise model is available, the designer want to keep it as simple as possible, considering the neglected dynamics as "uncertainty'.'
- The model used for control purpose is linearized around operating point, which would lead to uncertainty in case of deviation of operating point.
- Sometimes the non-modeled dynamics are unknown, and they can be considered as "hidden dynamics".

**Representing uncertainty:**
To take into account the model uncertainty, the following notations should be adopted

as:

$\Pi-$ a set of possible perturbed plant models.

$G(s) \in \Pi-$ nominal plant model, no uncertainty includes.

$G_p(s) \in \Pi-$ particular perturbed plant model.

The nominal plant $G(s)$ is the actual model of plant, what we assume that the plant is. Besides, $G_p(s)$ is used to denote a particular possible plant due to uncertainty, and then $\Pi$ represents the set of all possible plants. In detail, in Figure 3.2, the different

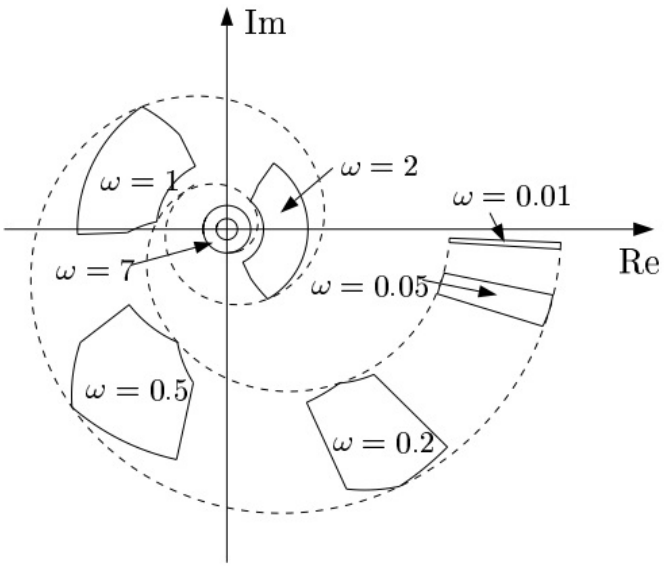


FIGURE 3.2: Uncertainty regions illustrated in the Nyquist plot at given frequency. Figure obtained from [1].

uncertainty sets corresponding to different frequencies $\omega$ are represented in Nyquist plot. These uncertainty regions generally have complicated shapes and complex mathematical descriptions, which results to obstacles in dealing with in the context of control system design.

There are different ways of representing uncertainties. However, this thesis will take into account only the multiplicative output uncertainty because of following reasons:

- First of all, the target of this thesis is to design the pre-compensator in order to deal with the interactions between inputs and outputs, which can be used in decentralized control synthesis.
- Secondly, output uncertainty is frequently less restrictive than input uncertainty in term of control performance.

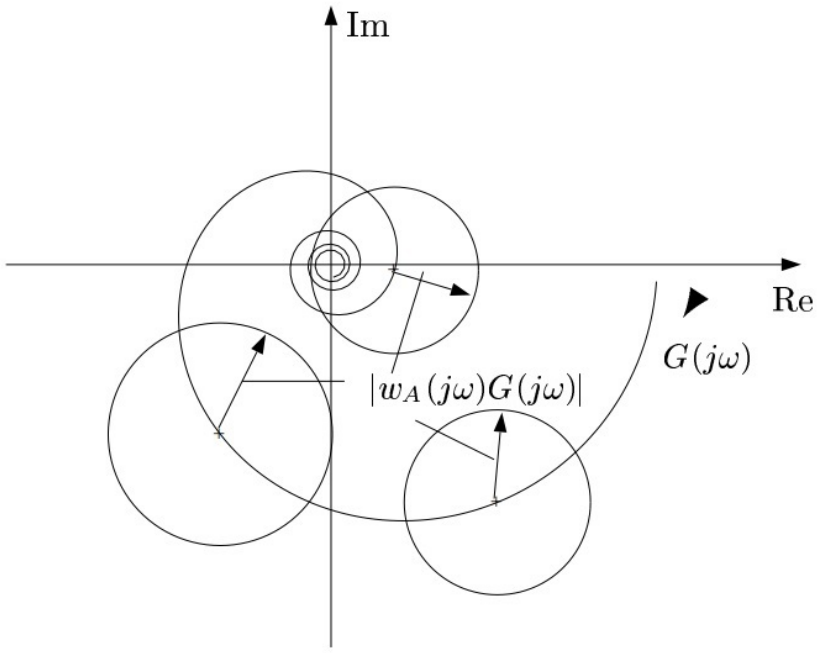


FIGURE 3.3: Disc-shaped uncertainty regions genereated by complex additive uncertainty. Figure obtained from [1].

For each frequency $\omega_i$, there exists a different uncertainty set $\Pi(\omega_i)$ with the multiplicative output uncertainty presentation for SISO plant as:

$$\Pi : G_p(s) = (1 + w_O(s)\Delta_O(s))G(s); \quad |\Delta_O(j\omega)| \leq 1, \forall\omega \tag{3.19}$$

where $w_O(s)$ is the scaling factor, it is a rational transfer function or can be seen as a weight which is introduced to normalize the perturbation to be less than 1 in magnitude $\forall\omega$; $\Delta_O(s)$ represents any stable transfer function with the magnitude less or equal than 1 $\forall\omega$. Then at each $\omega$, $\Delta_O(j\omega)$ generates a disc-shaped region centered at $(0, 0)$ with the radius 1, so $(1 + w_O(s)\Delta_O(s))G(s)$ represents a disc-shaped area centered at $G(j\omega)$ with radius $|G(j\omega)w_O(j\omega)|$ as shown in Figure 3.3.
In general, $w_O(j\omega)$ should be selected so that the uncertainty region $\Pi(\omega)$ has to be included in this region at each $\omega$. For simplicity, due to the dependence of $w_O(j\omega)$ to the nominal plant $G(j\omega)$, it is usually good to choose a simple nominal plan $G(j\omega)$ in order to achieve simple $w_O(j\omega)$, even if the uncertainty regions represented by $G_p(s)$ become larger than the need to include $\Pi$, or even if complicated dynamics are neglected.
Let start with the nominal MIMO plant with $m$ inputs and $p$ outputs represented as

follows:

$$G(s) = \begin{bmatrix} G^{(1,1)}(s) & G^{(1,2)}(s) & \dots & G^{(1,m)}(s) \\ G^{(2,1)}(s) & G^{(2,2)}(s) & \dots & G^{(2,m)}(s) \\ \vdots & \vdots & \ddots & \vdots \\ G^{(p,1)}(s) & G^{(p,2)}(s) & \dots & G^{(p,m)}(s) \end{bmatrix} \tag{3.20}$$

and the element by element multiplicative uncertainty of the form:

$$G_p(s) = (I + W_O(s)) \times G(s) \tag{3.21}$$

where $\times$ is Schur multiplier, which presents element by element multiplication, and $W_O(s)$ is defined as:

$$W_O(s) = \begin{bmatrix} w_O^{(1,1)}(s)\Delta^{(1,1)}(s) & \dots & w_O^{(1,m)}(s)\Delta^{(1,m)}(s) \\ w_O^{(2,1)}(s)\Delta^{(2,1)}(s) & \dots & w_O^{(2,m)}(s)\Delta^{(2,m)}(s) \\ \vdots & \ddots & \vdots \\ w_O^{(p,1)}(s)\Delta^{(p,1)}(s) & \dots & w_O^{(p,m)}(s)\Delta^{(p,m)}(s) \end{bmatrix} \tag{3.22}$$

$$|\Delta_O^{(i,j)}| \leq 1, \forall\omega, \quad i = 1, \dots, p \quad j = 1, \dots, m$$

Thus, the uncertainty set $\Pi$ represented by $G_p(s)$ is:

$$G_p^{(i,j)} = (1 + w_O^{(i.j)}\Delta_O^{(i,j)})G^{(i,j)}, \qquad |\Delta_O^{(i,j)}| \leq 1, \forall\omega \tag{3.23}$$

However, it is not feasible to present uncertainty in mentioned way due to the difficulty

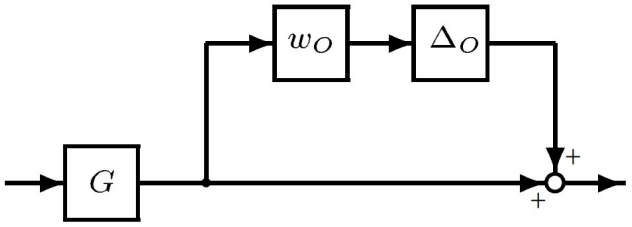


FIGURE 3.4: Multiplicative output uncertainty representation. Figure obtained from [1].

to quantify the magnitude of $w_O^{(i,j)}$. If all the elements $w_O^{(i,j)} \neq 0, \forall i, j$, then the uncertainty description is *full-block* ("unstructured"). It is obviously a poor assumption for multivariable plants. Therefore, only the diagonal output uncertainty, where $W_O(s)$ is diagonal matrix is considered. This uncertainty is frequently caused by uncertainty in particular output channels.

Now the uncertainty matrix $W_O(s)$ can be defined as:

$$W_O(s) = w_O(s)\Delta_O(s) \tag{3.24}$$

where the $\Delta_O(s)$ represents a specific source of uncertainty with $||\Delta_O||_\infty \leq 1$:

$$\Delta_O = \text{diag}[\Delta_i] = \begin{bmatrix} \Delta_1 & & & \\ & \ddots & & \\ & & \Delta_i & \\ & & & \ddots \end{bmatrix} \tag{3.25}$$

For the non-square plant with $m$ inputs and $p$ outputs, the size of $\Delta_O$ is $p \times p$. Similarly, $w_O$ is $p \times p$ matrix with the zero off-diagonal elements.

$$w_O = \text{diag}[w_{Oi}] = \begin{bmatrix} w_{O1} & & & \\ & \ddots & & \\ & & w_{Oi} & \\ & & & \ddots \end{bmatrix} \tag{3.26}$$

Actually, the diagonal uncertainty usually arises from a consideration of uncertainty or neglected dynamic in the particular output channels (sensors). If $\Delta_O$ is full matrix, then this will introduce non-physical couplings at the outputs of plant, resulting in a larger set of plant and robustness analysis which may be conservative (meaning the conclusion that the system may not meet its specification is wrong ). Eventually, the diagonal output uncertainty, as given in (3.25) and (3.26), has always to be considered due to the below reasons:

- It is always present and a system which is sensitive to this uncertainty will not work in practice.
- It often restricts achievable performance with multivariable control.

## 3.5 Conclusion

In this chapter, the basic notions about frequency response has been introduced. Besides, the T matrix algorithm is implemented to describe the frequency response of MIMO vibration system, which has been presented in adjacent section. Fortunately, T-matrix algorithm can be applied for square MIMO models as well as non-square MIMO plants. However, due to the complex in modelling and identification of frequency response, the uncertainty was introduced as multiplicative output uncertainty. This would lead to

some advantages as compared with the other representations of uncertainty. First of all, it is obviously benefit in designing the pre-compensator, which is able to counteract the interaction in MIMO plant. Moreover, the multiplicative output uncertainty is less restrictive than multiplicative input uncertainty in control performance point of view. After that, the lumped uncertainty was used in order to transform the completed additive uncertainty to the diagonal matrices. In the next chapter, the detailed information about pairing chosen and pre-compensator design will be discussed.

# Chapter 4

# Decoupling techniques

In this chapter, some pairing selection techniques would be proposed. They have been found very effective in MIMO decoupling control design. Hence, the chapter is structured as follows:

- **Singular Value Decomposition:** The formula and properties of SVD are presented, which is able to select the pairing between inputs and outputs of system.
- **Relative Gain Array:** An introduction of RGA and its properties are given. Its result in decentralizing the MIMO model hence is used to compares with the SVD.
- **Compensator Design:** Two compensators are designed based on the properties of RGA, which are able to transform the non-square MIMO model into square and diagonal dominant one.
- **Conclusion:** This section concludes the chapter.

## 4.1 Singular Value Decomposition

The Singular Value Decomposition (SVD) is one of the most important mathematical decompositions used in control design. It is a matrix decomposition used to determine if a system can be decoupled.

First of all, let consider the fixed frequency $\omega$ when $G(j\omega)$ is a constant $p \times m$ complex matrix, and denote that $G(j\omega)$ is $G$ for simplicity. Any complex matrix $G$ is generally decomposed into its singular value decomposition, as equation:

$$G = U\Sigma V^H \tag{4.1}$$

Where $U$ is an $p \times p$ orthogonal matrix whose columns are the eigenvectors of $GG^T$, $\Sigma$ is an $p \times m$ diagonal matrix with non-negative real numbers on the diagonal, denotes as $\sigma_i$, which are the positive square roots of the eigenvalues of $G^HG$ with $G^H$ be the complex conjugate transpose of $G$,

$$\sigma_i = \sqrt{\lambda_i(G^HG)} \tag{4.2}$$

and the $m \times m$ unitary matrix $V$ denotes the input singular vectors $v_i$.

### 4.1.1 Input and output directions

The *input direction* is represented by the column vectors $V$, denoted $v_i$, which are orthogonal and of unit length (orthogonal), as

$$||v_i||_2 = \sqrt{|v_{i1}|^2 + |v_{i2}|^2 + \cdots + |v_{ik}|^2} = 1 \tag{4.3}$$

$$v_i^H v_i = 1, \qquad v_i^H v_j = 0, \quad i \neq j \tag{4.4}$$

Similarly, the orthogonal and of unit length column vectors of $U$, denoted as $u_i$, represents the *output directions*. These input and output directions are derived from the singular values as

$$Gv_i = \sigma_i u_i \tag{4.5}$$

in which, $v_i$ and $u_i$ are vectors and $\sigma_i$ is a scalar. The above equation has been obtained from the equivalent description of equation (4.1) such as $GV = U\Sigma$ due to the definition $V$ is unitary, $V^HV = I$.

Therefore, the *input* can be considered in the direction $v_i$ as well as the *output* in the direction $u_i$. Consequently, the gain of matrix $G$ is given directly from the $i'$th singular value $\sigma_i$ as follows:

$$\sigma_i(G) = ||Gv_i||_2 = \frac{||Gv_i||_2}{||v_i||_2} \tag{4.6}$$

Hence, the SVD can gives some advantages as compared with another screening tools in term of eigenvalue decomposition for gain analysis and directionality of multivariable plants as

+ The singular values give better information about the gains of the plants.
+ The singular values give the orthogonal directions of plants.
+ The SVD is able to analyze also non-square plants.

### 4.1.2 Maximum and minimum singular values

It is obviously shown that the largest gain for *any* input directions is equal to the maximum singular value as

$$\bar{\sigma}(G) \triangleq \sigma_1(G) = \max_{d \neq 0} \frac{||Gd||_2}{||d||_2} = \frac{||Gv_1||_2}{||v_1||_2} \tag{4.7}$$

Similarly, the smallest gain for *any* input direction is obtained as

$$\underline{\sigma}(G) = \sigma_k(G) = \min_{d \neq 0} = \frac{||Gd||_2}{||d||_2} = \frac{||Gv_k||_2}{||v_k||_2} \tag{4.8}$$

where $k = \min(l, m)$. Hence, for any vector d which is not in the null space of $G$, the below condition is satisfied:

$$\underline{\sigma}(G) \leq \frac{||Gd||_2}{||d||_2} \leq \bar{\sigma}(G) \tag{4.9}$$

From the equation (4.5), and denote vector $\bar{v}$ as the largest amplitude input direction, $\bar{u}$ as output direction corresponding with the most effective inputs, we obtain

$$G\bar{v} = \bar{\sigma}\bar{u}, \qquad G\underline{v} = \underline{\sigma u} \tag{4.10}$$

### 4.1.3 Condition number

The condition number $\gamma$ of matrix $G$ is defined as the ratio between the largest and smallest singular values as

$$\gamma(G) \triangleq \frac{\bar{\sigma}(G)}{\underline{\sigma}(G)} \tag{4.11}$$

A matrix with a large condition number is called *ill-conditioned* (typically $\gamma > 10$), which means that some combinations of the inputs have a strong effect on the outputs while other combinations have much less effect. Therefore, the condition number can be used as a *controllability measure:*

- If $\gamma$ is small then the effects of uncertainty are not likely to be serious.
- If $\gamma$ is large, then there may be sensitivity to uncertainty.

On the other hand, the greater the $\gamma$ value, the harder it is for the system in question to be decoupled. As a rule of thumb, a system with a condition number $\gamma$ of more than 50 is difficult or impossible to decouple.

For example, in the worst case scenario for a two-input two-output MIMO system, using the exact same control variable twice would give a condition number $\gamma$ of $\infty$, because both manipulated variables would have the same effect on the controlled variables.

Hence, an ideal system would have a condition number $\gamma$ to equal to one, where each manipulated variable controls a single distinct output variable.

## 4.2 Relative Gain Array

### 4.2.1 Definition of RGA

The Relative Gain technique proposed firstly by Bristol in 1966 has not only become a valuable tool for screening selection of manipulative-controlled variables pairings, it has also been used to predict the behavior of controlled responses [16]. The analysis concerns around how to construct a *Relative Gain Array* (RGA). If $G$ is a non-singular square complex matrix $G$, then RGA is defined as:

$$RGA(G) = \Lambda(G) \triangleq G \times (G^{-1})^T \tag{4.12}$$

in which $\times$ denotes element-by-element multiplication (the Hadamard or Schur product). Now, consider the square MIMO plant with transfer function matrix $G(s)$ with element $g_{ij}(s)$ being particular transfer function from the input $u_j$ to output $y_i$. For simplicity, the Laplace variable $s$ would be omitted for $G(s)$ and $g_{ij}(s)$. The idea is to consider two extreme cases:

+ All other loops open: $u_k = 0, \forall k \neq j$
+ All other loops closed with perfect control: $y_k = 0, \forall k \neq i$

The *open loop gain* between input $u_j$ and output $y_i$, $g_{ij}$ can be evaluated when all the inputs except $u_j$ are assumed to be equal to zero:

$$\text{Other loops open :} \qquad \left(\frac{\partial y_i}{\partial u_j}\right)_{u_k=0,\forall k\neq j} \triangleq g_{ij} \tag{4.13}$$

In contrast, the *closed loop gain* $\hat{g}_{ij}$ is computed as follows if holding all outputs except $y_k$ constant and closing all other loops:

$$\text{Other loops closed :} \qquad \left(\frac{\partial y_i}{\partial u_j}\right)_{y_k=0,\forall k\neq i} \triangleq \hat{g}_{ij} \tag{4.14}$$

Basically, if no interaction between the loops are presented, the gain between input $u_j$ and output $y_i$ should remain the same when the other loops are closed, so that the *relative gain* $g_{ij}/\hat{g}_{ij} = 1$. On the other hand, $g_{ij}$ differs as compared with $\hat{g_{ij}}$ if there is

interaction in the system. Then the ratio

$$\lambda_{ij} \triangleq g_{ij}/\hat{g}_{ij} \tag{4.15}$$

could be used as an interaction measurement, and a *relative gain array* RGA with elements given by $\lambda_{ij}$ can be formed.
As can be seen from the definition of transfer function matrix, the relation $y = Gu$ leads to $g_{ij} = [G]_{ij}$ with $u_k = 0, k \neq j$, and similarly, $u = G^{-1}y$ gives

$$\left(\frac{\partial y_i}{\partial u_j}\right)_{y_k=0,\forall k\neq i} = [G^{-1}]_{ji} \tag{4.16}$$

Hence, the whole RGA matrix can be found directly from (4.12).

### 4.2.2 Algebraic Properties

The RGA matrix possesses several useful algebraic properties. Some of the most important are introduced as follows:

**Property 1:** If rows and columns are permuted in the transfer function matrix, $G$, then rows and columns in the RGA matrix are permuted in the same way.

**Property 2:** The division in (4.12) ensures the RGA matrix to be *scaling independent*, i.e.,

$$\Lambda(G) = \Lambda(S_1 G S_2) \tag{4.17}$$

with $S_1$ and $S_2$, diagonal scaling matrices with the same dimension as compared with $G$.

**Property 3:** The sum of elements in each row (and in each column) of the RGA is 1. This means, for $n \times n$ non-singular matrix $G$:

$$\sum_{i=1}^{n} \lambda_{ij} = \sum_{j=1}^{n} \lambda_{ij} = 1 \tag{4.18}$$

**Property 4:** If the transfer function matrix, G, is diagonal or triangular, and if the rows in the transfer function matrix are permuted to get nonzero elements along the diagonal in the case of a triangular G, then the RGA equals to the identity matrix. Hence, the RGA does not differ between diagonal and certain triangular models. It is clearly a drawback.

**Property 5:** For a $2 \times 2$ plant G, with nonzero elements only, the following holds: (a) If the number of positive elements in steady state condition is *odd* then $\lambda_{ij} \in (0, 1)$; (b) If the number of positive elements in steady state condition is *even* then $\lambda_{ij} \in (-\infty, 0) \cup (1, \infty)$.

The properties 1,2 and 4 are easily obtained by using the definition of the RGA matrix in equation (4.12). The rest, in the other hand is proven in [1].

### 4.2.3 Pairing recommendation

For example, let consider the RGA for the $2 \times 2$ transfer matrix:

$$G = \begin{bmatrix} g_{11} & g_{12} \\ g_{21} & g_{22} \end{bmatrix} \tag{4.19}$$

which can be generally computed as:

$$\Lambda(G) = \begin{bmatrix} \lambda_{11} & \lambda_{12} \\ \lambda_{21} & \lambda_{22} \end{bmatrix} \triangleq \begin{bmatrix} \lambda_{11} & 1-\lambda_{11} \\ 1-\lambda_{11} & \lambda_{11} \end{bmatrix} \tag{4.20}$$

where

$$\lambda_{11} = \frac{\text{“open-loop gain (with } u_2 = 0)\text{”}}{\text{“closed-loop gain(with } y_2 = 0)\text{”}} = \frac{1}{1 - \frac{g_{12}g_{21}}{g_{11}g_{22}}}$$

Depending on the value of $\lambda_{11}$, the following cases can be happened:

1. If $\lambda_{11} = 0$, indicates no interaction between input $u_1$ and output $y_1$. Hence, pairing should be chosen along the ani-diagonal, i.e. $u_1 - y_2, u_2 - y_1$.
2. If $\lambda_{11} = 1$, similar to above case, the pairing is chosen along the diagonal.
3. If $0 < \lambda_{11} < 1$, this case is not desirable since the gain increases (i.e. $g_{ij}$ increases) when the loops are closed. Hence, there are interactions in the system. Moreover, the worst case happens when $\lambda_{11} = 0.5$.
4. If $\lambda_{11} > 1$, now the gain degrades when the loops are closed. The interactions get worse the larger $\lambda_{11}$ is.
5. If $\lambda_{11} < 0$, now even the sign changes when the loops are closed and this is extremely undesirable. The more negative $\lambda$, the worse the interactions are.

Eventually, even for higher-dimension plants, the rule used to choose pairings is that corresponding RGA element is close to one. Definitively, negative pairings should be avoided.

### 4.2.4 The RGA-number

To characterize the chosen pairings with a simple measurement, the *RGA-number* can be used:

$$RGA \qquad number = ||\Lambda(S) - I||_{sum} \tag{4.21}$$

where the sum matrix norm is defined as $||A||_{sum} = \sum_{i,j}|a_{ij}|$ if the $n \times n$ matrix A has elements $a_{ij}, \quad i,j = 1,\dots n$. Clearly, the RGA-number measures how dominant the diagonal in the RGA is. A proper pairing choice should thus have a RGA-number close to zero.

### 4.2.5 Iterative RGA

Keep in mind that the disadvantage with the RGA number, at least for larger system, is that it needs to be recomputed for each alternative pairing. On the other hand, the RGA elements need to be computed only once. Hence, the iterative evaluation of the RGA has been proposed in order to select promising pairing for large system. Woff (1994) [17] found numerically that

$$\Lambda^{\infty} \triangleq \lim_{k\to\infty} \Lambda^{k}(G) \tag{4.22}$$

It has been proven that $\Lambda^{\infty}$ always converges to the identity matrix if G is a generalized diagonally dominant matrix. This property will be usefully in the following chapter.

### 4.2.6 A dynamic extension of the RGA

Bristol only used the plant at steady state condition, $G(0)$ when computing the RGA [16]. The reason for this, was probably that in the process industry this steady-state measurement is often far more easy to attain than the corresponding dynamic measurement, $G(j\omega)$. Fortunately, a dynamic extension of the RGA was proposed:

$$\Lambda(G(j\omega)) = G(j\omega) \times (G(j\omega)^{-1})^{T} \tag{4.23}$$

The definition is clearly same as compared with the original RGA, except that fact that the plant gain $G$, now ca be measured at any frequency $\omega$. Not surprisingly, the dynamic version of RGA have the same properties as the steady-state one. Hence, both of these RGA versions will be denoted as $\Lambda$.

When analyzing a system it is advisory to use this dynamic RGA and hence study the behavior of $\Lambda(G)$ in the interesting frequency range. As pointed out by Skogestad

and Postlethwaite, see[1], to avoid instability it is often sufficient to require $\Lambda(G)$ to be near the identity matrix at the crossover-frequency. However, a pairing that results to negative RGA-elements should not be tolerated for any frequency of interest.

### 4.2.7 Generalization for Non-square plants

The RGA can be adopted to use for $p \times m$ non-square plants, $G_{all}$ as follows:

$$\Lambda = G_{all} \times (G_{all}^{\dagger})^T \tag{4.24}$$

where † denotes the pseudo-inverse (Moore-Penrose inverse). Essentially, for the case of many candidate manipulations (inputs) one may consider not using those manipulations corresponding to columns in the RGA where the sum of the elements is much smaller than 1 (see [15]). Similarly for the case of many candidate measured outputs (or controlled outputs) one may consider not using those outputs corresponding to rows in the RGA where the sum of the elements is much smaller than 1.

Let $e_j = [0 \quad \cdots \quad 0 \quad 1 \quad 0 \quad \cdots \quad 0]^T$ be a unit column vector of length $m$, with value 1 at position $j$ and zeros in every other positions. Hence, the $j'$th input is $u_j = e_j^T u$. Similarly, define $e_i$ and achieve the $i'$th output $y_i = e_i^T y$. Then the following equations, if the plant either has full column rank or full row rank can be achieved for both two cases respectively [1]:

$$\sum_{j=1}^{m} \lambda_{ij} = ||e_i^T U_r||_2 \tag{4.25}$$

$$\sum_{i=1}^{p} \lambda_{ij} = ||e_j^T V_r||_2 \tag{4.26}$$

where $U_r$ and $V_r$ are matrices containing the first $r$ *output* and $r$ *input* singular vectors of $G_{all}$ respectively [1] Thus, $e_i^T U_r$ yields the projection of an unit output $y_i$ onto the effective output space of $G_{all}$, in the same way, $e_j^T V_r$ can be seen as the projection of an unit input on the effective input space of $G_{all}$ spanned by the columns of $V_r$.
Frequently, the selections of inputs and outputs for possible control scheme can grow rapidly with respect to a large group of candidates. Fortunately, the above results are obviously an efficient tool in the paring selection of inputs and outputs. If the desire is to eliminate some input candidate, the RGA for "full" transfer function matrix containing

[1]Input and output singular vectors can be obtained by performing the singular value decomposition of $G_{all}$ as follows:

$$G_{all} = U\Sigma V^H = U_r \Sigma_r V_r^H \tag{4.27}$$

where $\Sigma_r$ consists only of the $r$=rank($G$) nonzero singular values, $U_r$ consists of the $r$ first column of $U$, and $V_r$ consists of the $r$ first columns of $V$. As the conclusion in [1], the columns in $V_r$ represent the input directions that can effect the outputs, and similarly, the columns in $U_r$ represent the output directions which can be effected by the inputs.

every input and output candidates should be computed firstly, and then compute the column sums of the RGA. According to (4.26), those columns with sums lower than one is corresponding to inputs with a low impact of the system, which can be dismissed. Similarly, the selection of output candidates can be implemented based on the row sums of RGA and then, as a consequence of (4.25), outputs corresponding to low row sums can be removed.

However, it should be noticed that scaling independency is lost for a non-square model: For the case with more inputs than outputs, the RGA bases on *input scaling*, and in contrast, RGA will depend on *output scaling* (for detail, see [1]).

## 4.3 Compensator Design

In the multivariable control design framework, the simplest approach is to use diagonal controllers $K(s)$. This is often related to the assumption that the interaction between non-chosen pairing inputs and outputs of the plant can be neglected as compared with the pairing one. However, if the undiagnosed elements in $G(s)$ are large, it would lead to a bad performance of the closed-loop. Therefore, the alternative approach to deal with this problem is to use a compensator, which can reduce the interactions in the plant before designing controller. Fortunately, this technique is basically sufficient to use in the square-plant as well as the non-square plant.

Let start the simple feedback system in the Figure 4.1. A conceptual way is to use

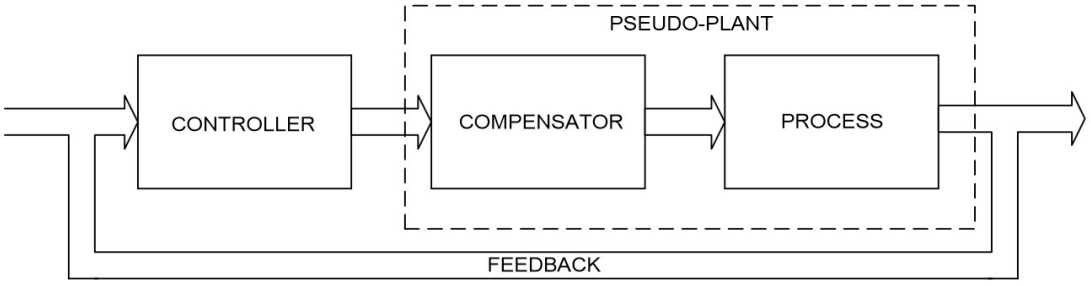


FIGURE 4.1: Pre-compensator for MIMO controller design.

pre-compensator, $W(s)$, which counteracts the interactions in the square plant $G(s)$ and results in the "compensated" plant as:

$$G_s(s) = G(s)W(s) \tag{4.28}$$

which is easier to control than the original square plant $G(s)$. After achieving the shaped plant $G_s(s)$, the diagonal controller is designed as follows:

$$K_s(s) = W(s)K(s) \tag{4.29}$$

Basically, the following assumptions are made according to the compensated plant $G_s(s)$:

- First of all, the dynamic decoupling system is attained when the overall plant is made to be diagonal at every frequency $\omega$. This can be done by using a pre-compensator of the form $W(s) = G^{-1}(s)G_{diagonal}(s)$, in which the diagonal elements in the shaped plant remain unchanged.
- If the overall plant is diagonal only in steady state ( $\omega = 0$), the decoupling is known as static. This may be obtained by selecting a constant pre-compensator matrix which is computed as $W = G^{-1}(0)$. Moreover, if the system is needed to be almost diagonal at a required frequency $\omega_0$, $G(0)$ in the aforementioned equation can be replaced by $G(j\omega_0)$. The bandwidth frequency is a good selection for $\omega_0$ as the effect of performance of reducing interaction is maximum in this frequency.

However, the decoupling control approach proposed above still has some limitations which can be found in detail in [1]. Some of the common strategies utilised in decoupling control are the internal control scheme (IMC) and partial decoupling of upper or lower triangular transfer function matrix.
On the other hand, even though the non-square plant can be decoupled by using compensator achieved from pseudo-inverse of $G(0)$, it still has some limitation based on not only the complicated selection of pairings but also in dealing with uncertainty of plants. More precisely, this thesis aims at solving the difficulties in pairing selection of a $4 \times 8$ non-square plant with following assumptions:

- The non-square plant has physical actuators (rear struts and anti-torque plate) which are located in the left and right side of the system. Actually, one output is affected by two actuators from left and right side with the similar significant transfer function in fixed frequency as compared with every other actuator. This mean that it is very difficult to tune the complex controller due to the strong multivarible property of the system. Moreover, actuators mounted in fuselage is expected to operate in combination to maximise their effect to the vibration attenuation. Hence,a compensator need to be developed, which is capable to transform the original plant to be square plant with diagonal dominant elements. The new inputs are called virtual inputs, whose quantities are equal the number of real outputs. Hence, the pair is only one virtual input and one output.

- On the other hand, the target of this thesis is to attenuate the vibratory components at the high frequency in the fuselage. As a consequence, the identified model is effected by the big uncertainty parts in term of the relative frequency or magnitude.

Let's start with the $p \times m$ non-square plant as:

$$G(s) = \begin{bmatrix} G^{(1,1)}(s) & \dots & G^{(1,m)}(s) \\ \vdots & \ddots & \vdots \\ G^{(p,1)}(s) & \dots & G^{(p,m)}(s) \end{bmatrix} \tag{4.30}$$

The compensator $W(s)$ is designed in such way that the following cost is minimized:

$$\min_{W(s)} J(s) = ||RGA(G_s(s)) - I||_\infty \tag{4.31}$$

in which, $I$ is identity matrix and $G_s(s) = G(s)W(s)$.

It is obviously realized that the size of $W(s)$ should be $m \times p$ and the $G_s(s)$ should be lower or upper triangular transfer function matrix, which can see in the algebraic properties $4^{th}$ of RGA. However, the obtained model $G_s(s)$ is a non-diagonal matrix which is undesirable from decentralized control design framework. This limitation can be overcome if a second compensator $W_s(s)$ is designed based on the compensated plant $G_s(s)$ in such a way:

$$W_s(s) = G_s(s)^{-1} G_s^{diag}(s) \tag{4.32}$$

with $G_s^{diag}$ is a diagonal matrix taken from the shaped transfer function matrix $G_s(s)$. Eventually, we are able to organize an **Algorithm 1** of compensator design as follows:

**Step 1:** Initialize the first compensator $W(s)$.

**Step 2:** Compute RGA matrix based on shaped plant and compare with identity matrix. Then the weighting function $W(s)$ should be modified in order to avoid the local minimization of the cost function.

**Step 3:** Update the new $W(s)$ and uses it as the new initialization compensator for next iterative.

Afterwards, go back to **Step 2**.

After that, the second compensator is achieved by using equation (4.32) and then the overall compensator is:

$$W_{overall}(s) = W(s)W_s(s) \tag{4.33}$$

However, even the idea of decoupling control is appealing, some comments carries out as follows:

- The compensator is designed by minimizing the cost function, it is impossible to ensure that the obtained minimization of cost function is global.
- The algorithm to find minimization of cost function is optimal approach, which can deal with only the fixed frequency $\omega$ as well as $G(j\omega)$. Then, there is no way to attain $W(j\omega)$ as the function of varying frequency, $W$ is achieved as constant matrix for each frequency $\omega$.

## 4.4 Conclusion

In conclusion, all necessary ingredients for decoupling control problem are presented. The two screening tools as SVD and RGA are introduced, which will be using to solving the pairing chosen in MIMO plants. However, due to some difficulties in the vibration model of helicopter system, the compensator design has been modified in order to achieve exactly diagonal shaped plants. It basic idea is to minimize the cost function between RGA of shaped plant and the identity matrix. In the next chapter, controller synthesis will be discussed.

# Chapter 5

# Controller design

The vibration model obtained in the identification step is MIMO, which can be decoupled by using the two compensators designed in Chapter 3. Our main goal of this chapter is to use control algorithms which are based on the LQR and $H_\infty$ approaches. Before starting developing the whole algorithms, theoretical background and technical considerations are presented. Hence, the chapter is structured as follows:

- **LQ-like cost controller:** LQR controller synthesis approach is introduced and will be applied to our compensated model.
- $H_\infty$ **active rotor control design:** The robust controller is designed for the MIMO model which has been described in the previous chapter.
- **Conclusion:** This section concludes the chapter.

## 5.1 LQ-like cost controller

Consider the compensated model obtained from previous step which is represented as linear model under the steady state conditions

$$y_N = T_{N,N} u_N + w \tag{5.1}$$

where $u \in \mathbb{R}^p$ is the vector of virtual manipulated variables, $y \in \mathbb{R}^p$ is the vector of controlled variables and $w$ represents the component of the vibration in frequency $\omega$ affecting in the system.

It has to be noted that the dynamics relating $u$ to $y$ can be assumed to be linear time-invariant ( which is a reasonable assumption if one considers a fixed steady flight

condition and a configuration for the vibration control system with actuators and sensors located in the fuselage) which is compensated by two compensators to be a diagonally dominant matrix, then the compensated frequency response matrix $G_s(j\omega)$ is described as

$$G_s(j\omega) = \begin{bmatrix} G_s^{(1,1)}(j\omega & & 0 \\ & \ddots & \\ 0 & & G_s^{(p,p)}(j\omega) \end{bmatrix} \tag{5.2}$$

where $G_s(j\omega) = G(j\omega)W(j\omega)W_s(j\omega)$, $W(j\omega)$ and $W_s(j\omega)$ are found from Chapter 3.

Therefore, the $T - matrix$ representation of the model will be

$$T_{N,N} = \begin{bmatrix} T_{N,N}^{(1,1)} & & 0 \\ & \ddots & \\ 0 & & T_{N,N}^{(p,p)} \end{bmatrix} \tag{5.3}$$

in which $T_{N,N}^{(i,j)}$ is obviously related to $G(j\omega)^{(i,j)}$ as

$$T_{N,N}^{(i,j)} = \begin{bmatrix} \text{Real}(G_s^{(i,j)}(j\omega) & \text{Imag}(G_s^{(i,j)}(j\omega)) \\ \text{-Imag}(G_s^{(i,j)}(j\omega)) & \text{Real}(G_s^{(i,j)}(j\omega)) \end{bmatrix} \tag{5.4}$$

The advantage of this approach using compensator is clearly that the non-square MIMO plant which is difficult to decouple has transformed to the diagonal dominance and square model. It results to the possibility of applying the decentralized controller for each SISO loop. Moreover, the uncertainties in off-diagonal elements of compensated model are degraded, which will effect slightly to the performance of LQ-like controller as well as $H_\infty$ controller.

Hence, from the definition of $T$-matrix algorithm, the discrete time relation for the reduction of the effect of $w$ on $y_N$ is given by

$$u_N(k+1) = u_N(k) - T_{N,N}^{-1} y_N(k) \tag{5.5}$$

with $k$ be the control cycle index.

On the other hand, the LQ-like cost function is defined for each discrete-time $k$ as

$$J(k) = y_N^T(k)Qy_N(k) + 2y_N^T(k)Su_N(k) + u_N^T(k)Ru_N(k) \tag{5.6}$$

where $Q = Q^T \geq 0, S + S^T > 0$ and $R + R^T > 0$. Replace $k$ by $k+1$ in (5.1) and subtracting the resulting equation (5.1) itself, yields the disturbance-free update model

$$y_N(k+1) = y_N(k) + T_{N,N}(u_N(k+1) - u_N(k)) \tag{5.7}$$

Substituting now $y_N(k)$ from (5.1) into (5.6) obtains a new cost function as

$$J(k) = u_N^T(k)Du_N(k) + 2u_N^T(k)T_{N,N}^T Qw(k) + w^T(k)Qw(k) \tag{5.8}$$

where $D = T_{N,N}^T QT_{N,N} + R$. The optimal control law is found by differentiating (5.8) with respect to $u_N(k)$

$$\frac{\partial J(k)}{\partial u_N(k)} = 2Du_N(k) + 2T_{N,N}^T Qw(k) \tag{5.9}$$

leading to the open-loop control algorithm

$$u_N(k+1) = -D^{-1}(T_{N,N}^T Q)w(k) \tag{5.10}$$

which can be equivalently written a closed-loop form as

$$u_N(k+1) = -T_{N,N}K_{N,N}u_N(k) + K_{N,N}y_N(k) \tag{5.11}$$

with

$$K_{N,N} = -D^{-1}(T_{N,N}^T Q). \tag{5.12}$$

From a practical point of view, the implementation of above discrete control algorithm has to include the following procedures:

(1) The determination on the component of $y$ in frequency $\omega$.

(2) The update of the component using equation (5.11) in frequency $\omega$.

(3) The determination of the time domain value of the control input $u$ via a modulation of the sine and cosine components in frequency $\omega$.

Note that if in the cost function (5.6) the weighting function matrices $Q$ and $R$ are chosen as the identity and zero matrices respectively, then the control law (5.11) reduces to (5.5).

The control law (5.11) can be rewritten as

$$u_N(k+1) = K_M u_N(k) + K_N y_N(k) \tag{5.13}$$

with $K_M = -T_{N,N}K_{N,N}$, $K_N = K_{N,N}$, $\quad K_{N,N}$ given by (5.12).

In this respect it is interesting to point out that the structure of matrix $T_{N,N}$ (see (5.4)) implies a similar structure of matrices $K_M$ and $K_N$. In detail, it is obviously that the

structure of every sub-matrix $T_{N,N}^{(i,j)}$ which is formulated as the form

$$T_{N,N}^{(i,j)} = \begin{cases} \begin{bmatrix} a^{(i,i)} & b^{(i,i)} \\ -b^{(i,i)} & a^{(i,i)} \end{bmatrix} & \text{if} \quad i = j, \quad i,j = 1 \cdots p \\ [0] & \text{if} \quad i \neq j, \quad i,j = 1 \cdots p \end{cases} \tag{5.14}$$

is extended to matrix $K_N$ ( its sub-matrices) by means of equation (5.10) and consequently $K_M$ also inherits the same type of structure. This means in the face of $2p.(2p+2p)$ entries in the matrices defining the control law, only $2p$ free parameters are exploited in the LQ control law.

The main drawback of the control law in equation (5.10) is that exact knowledge of $T$-matrix is assumed to be available. However, the erroneous model of it can not degrade only the performance of controller but make also the closed loop system to be unstable.. To address with model uncertainty, a *posteriori* analysis can be carried out to prove the robustness qualities. An interesting derivation from [18] provides upper bounds on the maximum singular value of the additive uncertainty for which robust stability is guaranteed by using the above described LQ-like control law. While such an analysis is of course informative, its main limitation lies in the difficulty in relating back bounds on the uncertainty on matrix $T_{N,N}$ to the actual model uncertainty in the dynamics of the helicopter. Based on these considerations, a robust framework could be used to design control law by incorporating all the uncertainties during the synthesis process. Conventional HHC control deals with performance degradation in presence of model uncertainty by introducing adaption, which takes into account the variation of the matrix $T_{N,N}$ between different flight conditions. Many different algorithms have been developed in this sense in the last few years, mainly based on the estimation of $T_{N,N}$ at specific time steps during the flight operations. In this respect, the interest in investigating a robust control design approach is motivated by the possibility to relax the need for continuous update of the $T$-matrix.

## 5.2 $H_\infty$ active control design

In this section an $H_\infty$ robust approach to the design of the HHC control law is presented.

### 5.2.1 Uncertainty model:

From the analysis carried out in Chapter 3 about the uncertainty representation, the multiplicative output uncertainty has been chosen

$$G_s(j\omega) = (I_p + W_O \Delta_O)\bar{G}(j\omega)W(j\omega)W_s(j\omega) \tag{5.15}$$

where two compensators $W(j\omega)$ and $W_s(j\omega)$ are designed based on the nominal plant $\bar{G}(j\omega)$, $I_p$ is the identity matrix of dimension $p$, $\Delta_O$ is a normalized representation of the uncertainty and $W_O$ represents the matrix of the uncertainty ellipsoids affecting the frequency response $\bar{G}^{(i,j)}(j\omega)$. It is clearly from the equation (5.15), no matter how the uncertainty representation is chosen, it will not affect to the way how to design compensators and the $T$-matrix algorithm. Eventually, the $T$-matrix representation of the plant illustrated in the Figure 5.1 will become

$$T_{N,N} = (I_{2p} + W_m \Delta)\bar{T}_{N,N}, \qquad ||\Delta||_\infty \leq 1 \tag{5.16}$$

in which, $I_{2p}$ is $2p \times 2p$ identity matrix, $W_m$ is defined as the $T$-matrix representation of $W_O$ and $\bar{T}_{N,N}$ is found in the equation (5.4). Therefore, $W_m$ is a diagonal matrix as

$$W_m = \text{blkdiag}(W_m^{(1)}, W_m^{(2)}, \ldots, W_m^{(p)}) \tag{5.17}$$

with

$$W_m^(i) = r^{(i)} \begin{bmatrix} \alpha^{(i)} & \beta^{(i)} \\ -\beta^{(i)} & \alpha^{(i)} \end{bmatrix}, \qquad i = 1, \ldots, p \tag{5.18}$$

with $r^{(i)}$ is a scalar scale factor and $\alpha, \beta$ are the parameter relating to the considered uncertainty of the specific output.

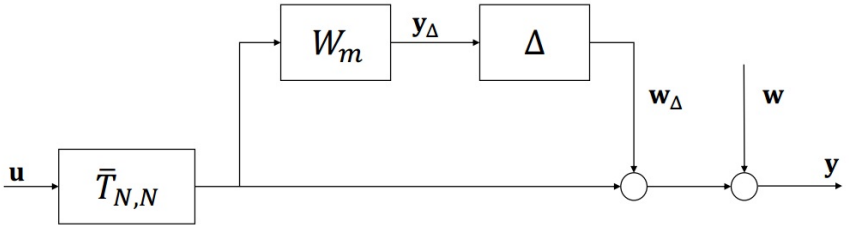


FIGURE 5.1: Block diagram of multiplicative output uncertainty.

On the other hand, the $\Delta$ is defined as

$$\Delta = \text{blkdiag}(I_2\delta^{(1)}, I_2\delta^{(2)}, \ldots, I_2\delta^{(p)}) \tag{5.19}$$

Then the block diagram of the uncertainty feedback system corresponding to the model (5.1), its uncertainty (5.16) and the controller (5.11) are depicted in the Figure 5.2.

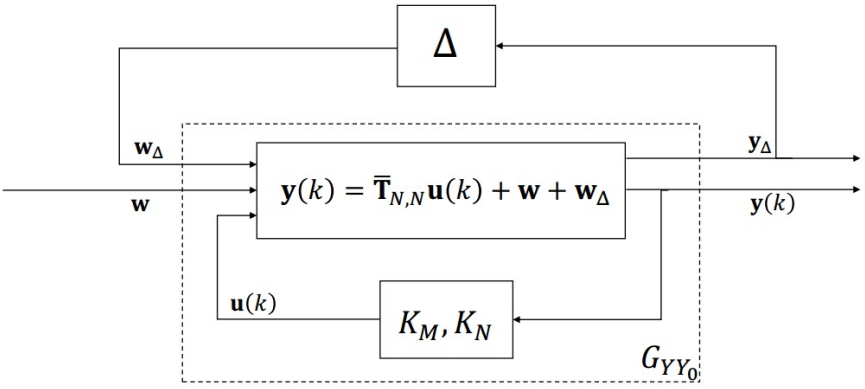


FIGURE 5.2: Block diagram of the closed loop of $H_\infty$ controller.

In Figure 5.2, variables $w_\Delta$ and $y_\Delta$ are defined as follows

$$\begin{aligned} y_\Delta(k) &= W_m \bar{T}_{N,N} u_N(k) \\ w_\Delta(k) &= \Delta y_\Delta(k) \end{aligned} \tag{5.20}$$

It results to the uncertain closed-loop system

$$\begin{aligned} u_N(k+1) &= K_M u_N(k) + K_N y_N(k) \\ y_N(k) &= \bar{T}_{N,N} u_N(k) + w(k) + w_\Delta(k) \\ y_\Delta(k) &= W_m \bar{T}_{N,N} u_N(k) \\ w_\Delta &= \Delta y_\Delta \end{aligned} \tag{5.21}$$

Letting $Y = [y_N \quad y_\Delta]^T$ and $Y_0 = [w \quad w_\Delta]^T$, the uncertainty model in (5.21) can be represented in the transfer function as

$$Y = G_{YY_0}(z) Y_0 \tag{5.22}$$

where $G_{YY_0}$ can be defined as

$$\begin{bmatrix} y \\ y_\Delta \end{bmatrix} = \begin{bmatrix} \bar{T}_{N,N}(zI - (K_M + K_N\bar{T}_{N,N}))^{-1} + I_{2p} & \bar{T}_{N,N}(zI - (K_M + K_N\bar{T}_{N,N}))^{-1}K_N + I_{2p} \\ W_m\bar{T}_{N,N}(zI - (K_M + K_N\bar{T}_{N,N}))^{-1}K_N & W_m\bar{T}_{N,N}(zI - (K_M + K_N\bar{T}_{N,N}))^{-1}K_N \end{bmatrix} \begin{bmatrix} w \\ w_\Delta \end{bmatrix} \tag{5.23}$$

### 5.2.2 $H_\infty$ control synthesis

Now, the next step of a $H_\infty$ controller synthesis problem is to define the weighting function $W_y^{(i)}, i = 1, \cdots, p$ and $W_u^{(j)}, j = 1, \cdots, p$ , respectively on the output $y_N$ and the virtual input variables $u_N$, which is depicted in the Figure 5.3. More precisely, the weighting function $W_y$ will be selected with assumption that the control design target is focused on the vibration attenuation at steady-state. Hence, the robust synthesis

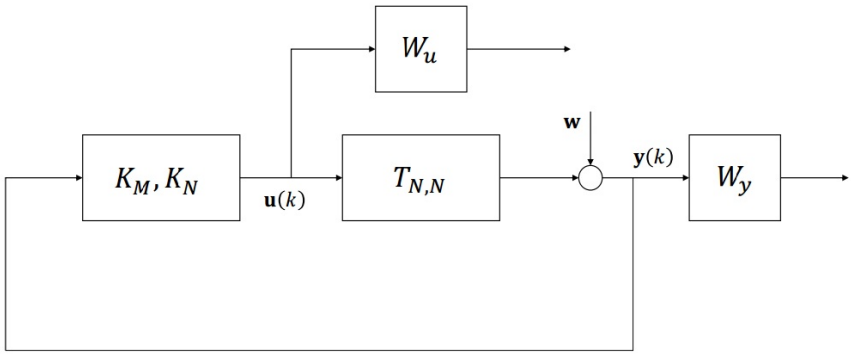


FIGURE 5.3: Augmented plant model

problem can be formulated as

$$\begin{aligned} &Find \quad K_M, K_N \\ &s.t. \\ &\left\| \begin{array}{c} G_{YY_0} W_y \\ G_{uy_0} W_u \end{array} \right\|_\infty \leq \gamma, \end{aligned} \tag{5.24}$$

where $G_{uy_0}$ is the control sensitivity function, obtained by re-opening the closed-loop from the disturbance $w$ to the control variable $u_N$ in the nominal case:

$$G_{uy_0} = (zI - (K_M + K_N \bar{T}_{N,N}))^{-1} K_N \tag{5.25}$$

The advantage of $H_\infty$ therefore as compared with LQ-like cost function approach is not only the possibility of dealing with the model uncertainty but also the additional benefit in control turning problem. Indeed, the vibration control problem is basically multivariable one, which the different locations in fuselage request different vibration reduction levels. From this viewpoint, the LQ-like, possibly adaptive, approach can turn out to be extremely time consumption. On the other hand, requirement specifications in terms of steady state vibration attenuation levels and desired transient performance can be immediately modified though the weighting function (see, *e.g*, Figure 5.4, which illustrates the suitable frequency response of continuous template weighting function

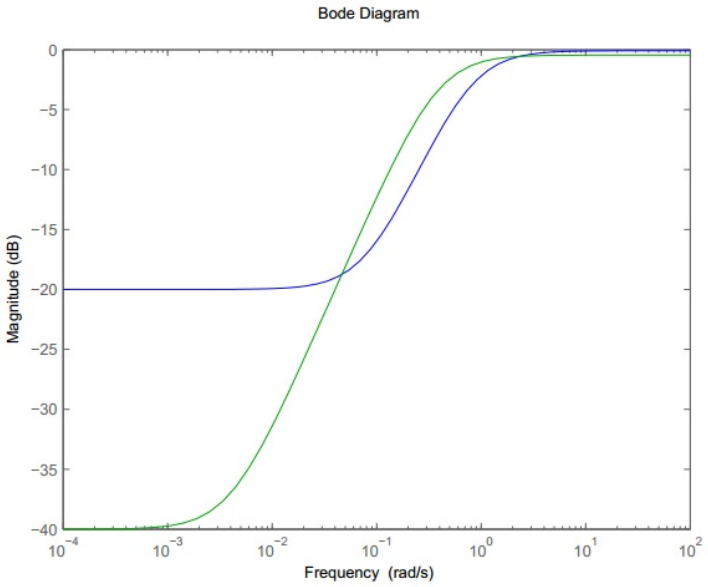


FIGURE 5.4: Frequency response of possible $W_y(s)$ weighting filter.

$W_y$), while the properties of the optimal solution can provide information about the actual distance between the desired and achievable performance. Moreover, the model used in this analysis is compensated to be transformed from non-square to square and diagonal dominance plant, which means that the decentralized controller with same weighting function for all SISO subsystem loops or higher penalties to specific outputs associated to more critical characteristics in terms of vibration (*e.g.*, pilot and co-pilot seats) can be considered.

### 5.2.3 Controller tuning

Problem (5.24) is a structured $H_\infty$ problem, which is known as both non-convex and non-smooth. This means that the convergence of the algorithm may depend on the initial controller and global optimality of the computed solution cannot guaranteed (for example, gradient-based descent algorithms could fail). In this viewpoint, a randomized method is capable to solve the optimization problem: the key point is that a optimal control law is achieved if the better control law cannot be found in its neighborhood (or, equivalently, can be found with null probability, [19]).

Hence, let's start with the assumption that the initial stabilizing controller based on the classical LQ and $T-$matrix is available. To compute the new controller $K^{(i+1)}$, the basic idea is to test randomly sample controllers in a neighborhood of $K^{(i)}$ and select the best one in terms of minimization of the cost function (5.24). If it is not longer

possible to find better controllers, the algorithm stops and the (local) optimal controller is obtained.

The stopping criterion is set on the parameter $0 < p^{max} < 1$, defined, in order to check the convergence, as the impossibility of finding better controller in the current iteration. The number $N_c$ of Monte Carlo samples and the initial step size $\lambda$ are also defined. Given a stabilizing initial controller $K^{(i)}$, the optimal controller is achieved by means of **Algorithm 2** (see [19]) for detail). Note that the term $\Delta K^{(i)}/\|\Delta K^{(i)}\|$ can be regarded as an approximation of the steepest descent direction, and the candidate controller $K^j$ is randomly generated regarding to the knowledge of the estimated steepest direction. Actually the controller is a random matrix, hence to check convergence the procedure is iterated as many times as the standard deviation in the cost function becomes below $\pm 1\%$, which guarantees the minimality of the cost with a very small tolerance.

Here is the detailed procedure of the **Algorithm 2** Tuning algorithm:

- **Step 1:** Generate $N_c$ controllers by means of a *Monte Carlo* generation: for $j = 1, \cdots, N_c$
$$K^{(j)} \leftarrow K^{(i)} + \lambda \|K^{(i)}\| \left( \eta^j + \frac{\Delta K^{(i)}}{\|\Delta K^{(i)}\|} \right)$$
- **Step 2:** Compute the $H_\infty$ norm $c^j \leftarrow J(K^{(i)})$
- **Step 3:** Select the candidate controller , $\hat{j} \leftarrow \min_i J(K^{(i)})$
- **Step 4:** Compute the an approximation of the rejection ratio $p^{(i+1)}$
- **Step 5: if** $\rho(G_{YY_0}) < 1$ $\triangleright$%check nominal and robust stability% set $K^{(i+1)} \leftarrow K^{\hat{j}}$ and $i \leftarrow i + 1$
**else** decrease step $\lambda$ and goto 1.
- **Step 6: if** $p^{(i+1)} > p^{(i)}$
decrease step $\lambda$
**else** increase step $\lambda$
- **Step 7: if** $p^{(i+1)} > p^{max}$
return $K$
**else** goto 1.

## 5.3 Conclusion

In this chapter, the problem of robust design of HHC control law has been considered. $H_\infty$ controller synthesis has been proposed and compared to the classical LQ solution.

Moreover, both controller have been developed based on the compensated plant achieved from previous Chapter. In the next chapter, simulations will be deployed and some comments will be made in term of performance of both approaches.

# Chapter 6

# Simulation result

In this chapter, a numerical example is used to illustrate the main properties of the proposed techniques. The $T-$ matrix considered in this example is based on the identified model from the paper [7]. More precisely, transfer function matrix is a 4x8 with 4 accelerometers and 8 actuators.
Hence, the chapter is structured as follows:

- **Singular Value Decomposition:** The result of paring selection based on SVD is proposed. Hence, the main drawback of this technique has been analyzed to show up the difficult of pairing selection.
- **Relative Gain Array:** This section presents the obtained results when RGA in pre-screening the inputs and then further controllability analysis is performed to non-square identified model.
- **Compensator Design:** Two compensators designed to transform the non-square model to the square and diagonal plant are proposed, which is main target of this thesis.
- **Controllers' performance comparison:** The simulation performances of both controllers are illustrated. In which, we have capability to evaluate the benefits of overall procedure.
- **Conclusion:** This section concludes the chapter.

## 6.1 Singular Value Decomposition

In this section, the numerical analysis based on SVD is proposed, which has been applied for the non-square model with the structure of sensors and actuators as above. For each

type of physical element (rear struts and anti-torque plate) two pairs of actuators have been chosen: one set up in the left side and one for the right side. So, AS07 and AS08 actuators are the left rear struts as compared with the right struts AD07 and AD08. On the other hand, for the left part of the anti-torque plate the actuators are TS05 and TS06 while for the right side they are TS03 and TD04. Hence, the actuators of each pair are in the same position but on opposite side: in this way, the way they are excited determines the type of deformation the structure is subject to.

The choice was taken in such way that each accelerometer is affected significantly by a pair of actuators. For example, accelerometer 2 is chosen as corresponding with the actuators TS05 and TS06 while the actuators AS07 and AS08 for accelerometer 9 and so on. In this way, accelerometer 2 works well with corresponding left actuators but not as well with others, which lead to the smaller inter-coupling effect.

As the result, the frequency response model was calculated at 1800 Hz, which is 4x8 complex value gain matrix. When the SVD is performed based on the following equation:

$$y = Gu = U\Sigma V^H u \tag{6.1}$$

Three obtained matrices are:

$$U = \begin{bmatrix} -0.9863 - 0.0000i & -0.1249 - 0.0000i & 0.0866 - 0.0000i & -0.0642 - 0.0000i \\ -0.0596 - 0.0637i & -0.0804 - 0.0987i & -0.6389 - 0.4437i & 0.2096 + 0.5721i \\ 0.0103 + 0.1342i & -0.5550 - 0.9794i & 0.0747 + 0.1060i & 0.0499 - 0.0134i \\ -0.0263 + 0.0284i & 0.0027 - 0.0761i & -0.5124 - 0.3289i & -0.2931 - 0.7322i \end{bmatrix} \tag{6.2a}$$

$$\Sigma = \Big[ diag\{1.4108, 0.5347, 0.1549, 0.0985\} | 0 \Big] \tag{6.2b}$$

$$V = \begin{bmatrix} -0.0130 - 0.0060i & -0.0070 + 0.0150i & 0.2020 + 0.5360i & 0.0330 - 0.1430i \\ 0.0240 + 0.0090i & -0.0050 + 0.0410i & 0.1430 + 0.6860i & 0.1170 - 0.2220i \\ 0.2700 + 0.5890i & 0.2280 - 0.1380i & 0.0320 + 0.1990i & -0.0130 + 0.0120i \\ -0.1850 - 0.6860i & -0.0950 - 0.1130i & -0.0240 + 0.1890i & 0.0530 + 0.0230i \\ -0.0330 + 0.0080i & 0.1300 - 0.2200i & -0.0900 - 0.1310i & 0.2550 - 0.5140i \\ 0.0120 - 0.0040i & 0.1410 - 0.1530i & -0.0283 - 0.1890i & 0.3560 - 0.5540i \\ -0.1010 + 0.1030i & -0.0670 - 0.6480i & 0.0270 + 0.1550i & 0.0670 + 0.3800i \\ -0.2140 + 0.0750i & -0.1510 - 0.5900i & 0.0500 - 0.1240i & 0.0260 + 0.0040i \end{bmatrix} \tag{6.2c}$$

The first thing needed to be considered is the condition number:

$$CN = \frac{\sigma_{max}}{\sigma_{min}} = 14.32 \tag{6.3}$$

which means that the largest singular value is more than 10 times larger than the smallest one. If a control variable has the main component that is going to be multiplied by the smallest singular value, than it is clear that this control variable has a much smaller effect than the others.

The SVD gives information about the possible pairings among the channels: suppose we want to pair the measured variables with the control variables, this is done in the following way: the measurement variable corresponding to the largest element of the first column of matrix U is taken and it is paired with the control variable corresponding to the largest element of the first vector of matrix V. The same is done for the other columns.

In our case the V and U matrices are complex value so we take the absolute values:

$$abs(U) = \begin{bmatrix} 0.9863 & 0.1247 & 0.0866 & 0.0642 \\ 0.0872 & 0.1273 & 0.7778 & 0.6092 \\ 0.1346 & 0.9810 & 0.1297 & 0.0517 \\ 0.0387 & 0.0761 & 0.6088 & 0.7887 \end{bmatrix} \tag{6.4a}$$

$$abs(V) = \begin{bmatrix} 0.0143 & 0.0166 & 0.5728 & 0.1468 & 0.0671 & 0.1305 & 0.6915 & 0.3874 \\ 0.0256 & 0.0413 & 0.7007 & 0.2509 & 0.2472 & 0.2643 & 0.4313 & 0.3555 \\ 0.6479 & 0.2665 & 0.2016 & 0.0177 & 0.4195 & 0.4673 & 0.0632 & 0.2627 \\ 0.7105 & 0.1476 & 0.1905 & 0.0578 & 0.4239 & 0.4392 & 0.0642 & 0.2381 \\ 0.0340 & 0.2555 & 0.1589 & 0.5738 & 0.5750 & 0.4666 & 0.0738 & 0.1570 \\ 0.0126 & 0.2081 & 0.1911 & 0.6585 & 0.4505 & 0.4923 & 0.1690 & 0.1114 \\ 0.1443 & 0.6515 & 0.1573 & 0.3859 & 0.0889 & 0.1177 & 0.3335 & 0.4972 \\ 0.2268 & 0.6090 & 0.1337 & 0.0263 & 0.1933 & 0.1657 & 0.4258 & 0.5583 \end{bmatrix} \tag{6.4b}$$

Now, the largest element of the first column of $abs(U)$ is the first, corresponding to the first accelerometer chosen (which is accelerometer 2 ); we expect that this accelerometer couples well to the left actuators of the anti-torque plate. Inspecting the second matrix, the largest element is the fourth (corresponding to actuator TS06). However the third element which has a value of 0.65 is really close to the previous one: this element correspond to the actuator TS05. The other elements of the first column of $abs(V)$ have a value that can be neglected when compared to these. Consider now the second column of matrix $abs(U)$: the element with the largest value is the third (0.98) corresponding to accelerometer 10. Looking at the second column of matrix $abs(V)$, the element with the largest value is the seventh (0.65), which correspond to the actuator TD03 but again its paired actuator TD04 has a value (0.6) that is close to it, meaning that these two actuators are significant for this accelerometer.

| Accelerometer | Actuators |
|---|---|
| 2 | TS05, TS06 |
| 9 | AS07, AS08 |
| 10 | TD03, TD04 |
| 18 | AD07, AD08 |

TABLE 6.1: Paring selection between the actuators and accelerometers based on SVD technique.

Going on, for the third column of $abs(U)$ the largest value 0.7778 corresponding to accelerometer 9: inspecting the third column of the other matrix the largest value is 0.7 which correspond to the actuator AS08, but also the first element (actuator AS07) has a significant value: the other values are much smaller than these hence they are not significant.

Finally the last column of $abs(U)$ has as largest value 0.7887 which corresponds to accelerometer 18. Analyzing the fourth column of matrix $abs(V)$ the element with the largest element is the sixth (0.658) but again also the seventh element has an important value (0.57) significantly bigger than the others: these correspond to the actuators AD07 and AD08.

Note that there are 2 values in the $U$ matrix that are not the maximal of their corresponding columns but can be compared to them: these are the (4,3) and (2,4) elements: these might tell us tell us that accelerometer 9 is also significant for the actuators AD07 and AD08 and that accelerometer 18 is significant for the actuators AS07 and AS08. Finally, the Table 6.1 shows the optimal pairings selected from SVD approach.

Another thing to point out is that from this analysis it seems the inter-channel coupling effect of a chosen subsystem is not so important. Actually this is in general not true and it depends strictly on the choice of accelerometers: accelerometers chosen in this case, for their positions in the cabin, are significant almost for only a group of actuators (accelerometer 9 for the actuators of the left rear strut, the 18 for the actuators of the right rear strut and so on).

## 6.2 Relative Gain Array

In this section, a method to combine inputs-outputs structure is adopted. This method uses the RGA to pre-screen the inputs and further controllability analysis is performed to select the best control structure. In 1995, Cao [15] considered the selection of manipulations in a chemical process for the hydrodealkylation of toluene (*HDA process*). The plant has 5 controlled outputs and 13 candidate manipulators. His aim was to select

the combination of 5 inputs and 5 outputs in such a way that the RGA matrix of this structure is closed to identity matrix as much as possible.

Similarly, in this thesis, the manipulated variables need to be chosen from 8 candidate inputs, $u_1, u_2, \cdots, u_8$. Clearly, there exist $\binom{8}{4} = 70$ combinations with 4 inputs and 4 outputs. At steady state 1800 Hz, the numerical transfer function matrix is:

$$G_{all}^T = \begin{bmatrix} 0.0211 + 0.0154i & -0.0631 - 0.0457i & 0.0044 - 0.0035i & -0.0344 - 0.0253i \\ -0.0319 - 0.0047i & -0.0762 - 0.0699i & -0.0041 - 0.0145i & -0.0359 - 0.0338i \\ -0.3904 - 0.8078i & -0.0946 - 0.0238i & 0.1236 + 0.1196i & 0.0064 - 0.0390i \\ 0.2631 + 0.9645i & 0.0790 + 0.0180i & -0.0421 + 0.0116i & -0.0271 + 0.0158i \\ 0.0344 + 0.0051i & 0.0023 - 0.0055i & 0.0764 + 0.1375i & 0.0542 + 0.0450i \\ -0.0287 + 0.0168i & -0.0067 + 0.0007i & 0.0367 + 0.1129i & 0.0474 + 0.0604i \\ 0.1450 - 0.1004i & 0.0458 - 0.0028i & 0.3799 + 0.1811i & -0.0052 - 0.0205i \\ 0.3084 - 0.0666i & 0.0532 + 0.0062i & 0.3635 + 0.1354i & 0.0360 + 0.0129i \end{bmatrix} \tag{6.5}$$

and the corresponding RGA-matrix is

$$\Lambda^T = \begin{bmatrix} 0.0076 - 0.0068i & 0.2956 + 0.0102i & 0.0008 - 0.0022i & 0.0459 - 0.0012i \\ -0.0011 + 0.0159i & 0.5259 - 0.0180i & -0.0061 - 0.0045i & 0.0374 + 0.0066i \\ 0.3391 + 0.0611i & 0.0841 - 0.0385i & 0.0853 - 0.0493i & 0.0237 + 0.0267i \\ 0.5937 - 0.0698i & -0.0301 + 0.0826i & -0.0091 + 0.0067i & 0.0122 - 0.0195i \\ -0.0070 - 0.0114i & 0.0084 + 0.0145i & 0.0544 + 0.0324i & 0.3650 - 0.0354i \\ 0.0137 + 0.0030i & 0.0104 - 0.0180i & 0.0249 + 0.0308i & 0.4645 - 0.0159i \\ 0.0120 + 0.0179i & 0.0849 - 0.0031i & 0.4829 - 0.0783i & 0.0394 + 0.0635i \\ 0.0420 - 0.0100i & 0.0207 - 0.0298i & 0.3668 + 0.0645i & 0.0119 - 0.0247i \end{bmatrix} \tag{6.6}$$

As matrix $\Lambda^T$ is complex valued matrix, the absolute value is studied:

$$abs(\Lambda^T) = \begin{bmatrix} 0.0101 & 0.2958 & 0.0023 & 0.0460 \\ 0.0159 & 0.5261 & 0.0075 & 0.0380 \\ 0.3447 & 0.0926 & 0.0985 & 0.0355 \\ 0.5977 & 0.0880 & 0.0112 & 0.0229 \\ 0.0133 & 0.0167 & 0.0634 & 0.3666 \\ 0.0140 & 0.0207 & 0.0396 & 0.4652 \\ 0.0217 & 0.0851 & 0.4892 & 0.0747 \\ 0.0432 & 0.0362 & 0.3725 & 0.0273 \end{bmatrix} \tag{6.7}$$

Obviously, the RGA can give information about the possibility in choosing the pairing of the system. It follows the rule in such way that the element in RGA matrix corresponding

with the input should be chosen as non negative and close to 1. On the other hand, the properties of RGA matrix used in choosing the pairing of inputs-outputs are $3^{rd}$ and $5^{rd}$ in 4.2.

From the above matrix, one could say that the largest element in the first column of $abs(\Lambda^T)$ is the fourth, which is corresponding with actuator TS06. The chosen accelerometer to be controller by TS 06 is 2. However, it is clear that the third element of $abs(\Lambda^T)$ is also very closed to the largest one, corresponding to actuator TS05. Hence, accelerometer 2 can be controlled by both chosen actuator which have significantly impact as compared with the rest in the first column.

When moving to the second column of matrix $abs(\Lambda^T)$, it shows that the actuator AS08 corresponding to the second element influences strongly to accelerometer 9 but again the first element also is big, which would lead to the fact that actuator AS07 and AS08 can be considered as the controller's inputs to the output accelerometer 9. The others are neglected in comparing the previous actuators.

Thirdly, the largest element in the $3^{rd}$ column of matrix $abs(\lambda^T)$ is 0.4892, corresponding to the actuator TD03, while the next significant element is the last one ( actuator TD04). Moreover, the rest are neglected because of the tiny impact to accelerometer 10.

Finally, the last accelerometer 18 is controlled by the actuator AD08 and AD 07 which correspond to the sixth and fifth elements of $4^{th}$ column of matrix $abs(\Lambda^T)$, respectively. However, the RGA has another benefit as compared with the SVD approach in selecting the input-output pairing of the model. As the above analysis, the RGA and SVD give the same results in which one accelerometer is effected strongly by two actuators. Moreover, the obtained result can be confirmed again to understand more clearly by iterative evaluation of the RGA which was introduced in chapter 4. Applying this approach, the RGA matrix will be computed repeatedly and then finally provided the most significant interaction between inputs and one output. Let's compute $(\Lambda^T)^8$ to obtain:

$$(\Lambda^T)^8 = \begin{bmatrix} 0.0000 - 0.0000i & 0.0000 - 0.0000i & 0.0000 - 0.0000i & 0.0000 + 0.0000i \\ 0.0000 - 0.0000i & 1.0000 + 0.0000i & -0.0000 - 0.0000i & -0.0000 - 0.0000i \\ 0.0000 - 0.0000i & 0.0000 + 0.0000i & 0.0000 + 0.0000i & 0.0000 + 0.0000i \\ 1.0000 - 0.0000i & -0.0000 + 0.0000i & 0.0000 + 0.0000i & 0.0000 - 0.0000i \\ 0.0000 - 0.0000i & -0.0000 + 0.0000i & -0.0000 + 0.0000i & 0.0000 - 0.0000i \\ 0.0000 - 0.0000i & -0.0000 + 0.0000i & 0.0000 + 0.0000i & 1.0000 - 0.0000i \\ 0.0000 - 0.0000i & -0.0000 - 0.0000i & 1.0000 - 0.0000i & 0.0000 - 0.0000i \\ 0.0000 - 0.0000i & -0.0000 - 0.0000i & 0.0000 - 0.0000i & 0.0000 + 0.0000i \end{bmatrix} \tag{6.8}$$

| Accelerometer | Actuators |
|---|---|
| 2 | TS05, TS06 |
| 9 | AS07, AS08 |
| 10 | TD03, TD04 |
| 18 | AD07, AD08 |

TABLE 6.2: Paring selection between actuators and accelerometers based on RGA technique.

We find from each column of the steady-state RGA matrix given in $(\Lambda^T)^8$ that there are 4 elements which have the absolute value is 1 while the rest have 0 absolute values. their positions are $4^{th}$ in $1^{st}$ column, $2^{nd}$ in second column, $7^{th}$ in the third column and $6^{th}$ in the last one. Eventually, it is obviously that we have same result in pairing selection in both techniques RGA and SVD, is illustrated in Table 6.2. For each output, the control structure can select two manipulated actuators with significant impact as compared with the others even though the RGA technique has the capability to select the best pairing for each output by using iterative evaluation.

In this experiment, actuators are mounted in the helicopter in such a way that they can be effectively operated simultaneously to maximise their effect to reduce the noise. However, this combination would lead to a fact that the controllers are very complex and difficult to tune. Hence, both approaches SVD and RGA are not able to use for this kind of model. We will propose the automatic design approach to reduce the number of actual control inputs by using pre-compensators.

## 6.3 Compensator design

The main drawbacks of two above approaches is the difficulty in selecting the pairings between inputs-outputs. It is obvious that one output can be effected strongly by two inputs. In the other hand, the classical way to make the simplification from MIMO model to multi SISO case is adapted to find the new set of independent inputs and outputs. The goal of this step is to eliminate the interactions so that a change in one system variable will not cause corresponding changes in the other system variables. Moreover, this classical approach is used only in the square system with the full information about input-output pairings. As a consequence, it is not suitable for applying in non-square system with non selection in pre-screening.

Hence, in this thesis, the new technique will be proposed in order to obtain the optimal solution for decentralized controller in multivariable design. The MIMO model of the vibration in helicopter is derived in previous section with 8 inputs and 4 outputs. The

idea is to design a compensator which is able to transform the model into a diagonally dominant system.

Applying **Algorithm 1** proposed in the previous chapter, the first compensator is attained as follows:

$$C_{RGA} = \begin{bmatrix} 0.0000 & 3.2820 & -0.5276 & -12.7469 \\ 0.7749 & -5.2440 & -1.6056 & 4.2976 \\ -0.6464 & 1.6168 & -1.7409 & -3.0630 \\ 0.0111 & 1.2459 & -1.9486 & -5.5845 \\ 1.6501 & -1.1188 & 0.1784 & 44.8798 \\ -1.2287 & -0.4669 & -5.1674 & -9.0508 \\ -0.0164 & -0.9064 & -8.4363 & -19.7484 \\ 0.0245 & 0.7250 & 2.0410 & 8.5225 \end{bmatrix} \tag{6.9}$$

In this algorithm, we used a nonlinear optimization solver **fminsearch** in MATLAB optimization toolbox for implementing **Algorithm 1**. The default option interior point method is chosen. In order to avoid local minima, the optimal compensator of the previous iteration step is set as initial value of next iteration step.

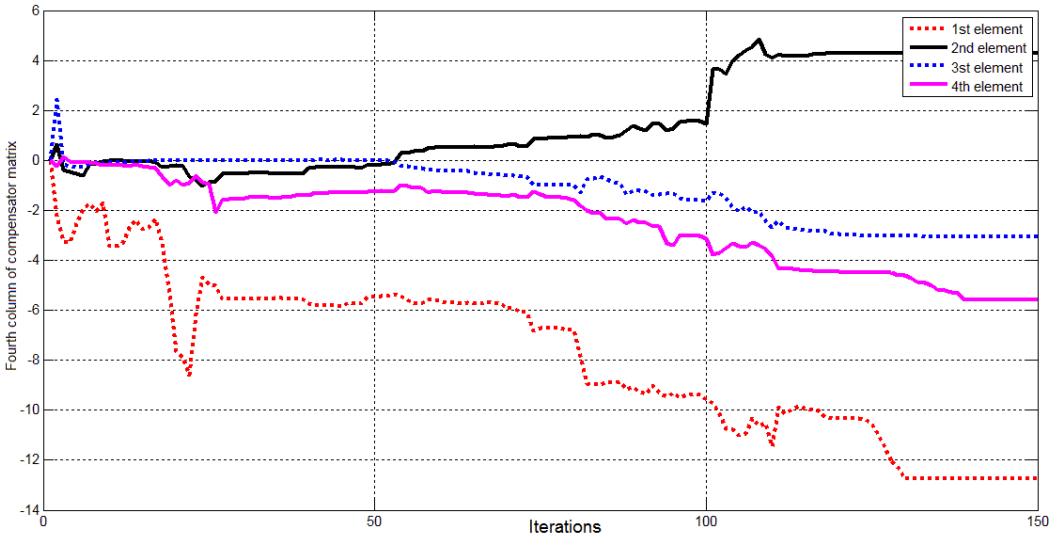


FIGURE 6.1: The iteration convergence of the fourth column of the first compensator elements.

The convergence of elements in fourth column of compensator matrix have been shown in Figure 6.1. The dash dot red line corresponds to the value of the 1st element in 4rd column of matrix $C_{RGA}$, while the solid black line present the second element and similarly with the dash dot blue line for the third element and the solid pink line for 4rd

one. As illustrated in Figure 6.1, they converges to the optimal solution after at least 140 iterations with 10 seconds for each iteration in average. This mean the approach is time consumption in term of convergence rate. And hence this technique can not be used to design the optimal compensator for fast dynamic system.

As we can see from the 6.10, the achieved compensated model is basically lower triangular, which can be used in designing the second compensator to obtain diagonally dominant system based on the property $3^{st}$ of RGA's algebraic properties in Chapter 4.//

$$G_{RGA} = \begin{bmatrix} 0.3278 - 0.5170i & 0.0002 + 0.0000i & -0.2323 - 0.1515i & 0.8889 + 1.6365i \\ 0.0156 + 0.0483i & 0.1356 - 0.2134i & -0.0764 - 0.1744i & 0.0382 - 0.1095i \\ 0.0001 - 0.0001i & -0.0001 + 0.0002i & -2.7679 + 2.0160i & -1.5250 - 2.2778i \\ -0.0001 + 0.0001i & -0.0000 - 0.0002i & -0.0005 + 0.0001i & 2.8289 - 2.1962i \end{bmatrix} \tag{6.10}$$

In 6.10, it is obvious that the 2nd element of the first column is not exactly zero, equal to $0.0156 + 0.0483i$. But it is acceptable if we compare the module of this element to the diagonal elements. And in the next result, it will be shown that this element does not effect to the performance of the whole system.

On the other hand, the below matrix represents the RGA number matrix of $G_{RGA}$ in which we can easily recognize that RGA matrix is closed to identity matrix. As a result, the input-output couple selections are optimal with diagonal pairings.

$$RGA_{Number} = \begin{bmatrix} 1.0000 - 0.0001i & 0.0001 + 0.0000i & -0.0000 - 0.0000i & -0.0001 + 0.0001i \\ 0.0000 + 0.0000i & 0.9999 - 0.0001i & 0.0000 + 0.0000i & -0.0000 + 0.0000i \\ -0.0000 - 0.0000i & -0.0000 + 0.0000i & 1.0000 - 0.0001i & -0.0000 + 0.0001i \\ -0.0001 + 0.0001i & -0.0000 + 0.0000i & -0.0001 + 0.0001i & 1.0001 - 0.0002i \end{bmatrix} \tag{6.11}$$

The next step is to design the second compensator which helps us to split the achieved system into four independent SISO control loops working in parallel. It is clear that this compensator is obtained from the equation $C_{DIG} = G_{RGA}^{-1}\text{diag}(G_{RGA})$, in which $\text{diag}(G_{RGA})$ is a matrix with only the diagonal elements of $G_{RGA}$

$$C_{DIG} = \begin{bmatrix} 1.0000 & 0 & -0.0058 + 0.4519i & 1.8430 - 2.6446i \\ 0.1282 - 0.1545i & 1.0000 & -0.3514 + 0.6836i & -0.1274 - 0.1640i \\ 0 & 0 & 1.0000 & 0.0314 - 0.7996i \\ 0 & 0 & 0 & 1.0000 \end{bmatrix} \tag{6.12}$$

The second compensator can always be attained because the $G_{RGA}$ is always invertible. Hence the total compensator will be

$$C_{Total} = \begin{bmatrix} 0.4208 - 0.5071i & 3.2820 & -1.6809 + 2.2436i & -13.1816 - 0.1164i \\ 0.1026 + 0.8102i & -5.2440 & 0.2326 - 3.2346i & 6.3434 + 0.0946i \\ -0.4391 - 0.2498i & 1.6168 & -2.3053 + 0.8131i & -4.5150 + 2.8363i \\ 0.1708 - 0.1925i & 1.2459 & -2.3865 + 0.8567i & -5.7840 + 1.3244i \\ 1.5067 + 0.1729i & -1.1188 & 0.5620 - 0.0191i & 48.0691 - 4.3230i \\ -1.2886 + 0.0721i & -0.4669 & -4.9962 - 0.8744i & -11.4181 + 7.4578i \\ -0.1326 + 0.1400i & -0.9064 & -8.1177 - 0.6270i & -19.9280 + 6.9377i \\ 0.1174 - 0.1120i & 0.725 & 1.7861 + 0.5067i & 8.5394 - 1.8157i \end{bmatrix} \tag{6.13}$$

which comes from the equation $C_{Total} = C_{RGA}C_{DIG}$. Then the diagonal system is obtained as follows

$$G_{Final} = \begin{bmatrix} 0.3278 - 0.5170i & 0.0002 + 0.0000i & -0.0007 - 0.0002i & -0.0028 - 0.0022i \\ -0.0000 + 0.0000i & 0.1356 - 0.2134i & -0.0001 + 0.0000i & 0.0006 - 0.0010i \\ 0.0001 - 0.0001i & -0.0001 + 0.0002i & -2.7680 + 2.0160i & 0.0001 - 0.0018i \\ -0.0001 + 0.0001i & -0.0000 - 0.0002i & -0.0004 + 0.0001i & 2.8291 - 2.1953i \end{bmatrix} \tag{6.14}$$

Theoretically, nothing can be said about the natural convergence of the first compensator due to the optimization solver used in this thesis. All the elements of the first compensator are expected to converge simultaneously, then the number of variables of nonlinear function are 32 (4x8). In addition, Skogestad and Postlethwaite [1] have noticed that the RGA of a triangular plant is always the identity matrix ( $\Lambda = I$) or equivalently the RGA number is zero. The reverse is also true; that is, an identity RGA matrix ($\Lambda(G) = I$) implies that G is triangular, which holds only for 3x3 systems or smaller. For a 4x4 or higher order, the condition is not always true. Hence, the $\Lambda = I$ would be preferred but the plant might not be triangular. It has shown in $G_{RGA}$ with non-zero element in position (2,1).

## 6.4 Controller

We want to demonstrate the capabilities of the proposed robust HHC scheme for the compensated plant. Each controller element $k_i$ of LQ-like cost and robust controller is designed based on the corresponding diagonal element of $G_{Final}$ in the previous section, such that each individual loop is stable. The control input of each loop now is a virtual input, which will change the behavior of all actuators via two proposed compensators as aforementioned. In addition, it is expected that the robust HHC controller will

outperform the classical LQ-like cost controller. In this section, simulation results show the vibration attenuation performance as well as the settling time $T_s$.

The system now contains four feedback loops with the transfer function as

$$y = G_{Final}u \tag{6.15}$$

where $u = [u_1 \quad u_2 \quad u_3 \quad u_4]$ is defined as the virtual inputs of the new system, and $y$ are four accelerometers 2, 9, 10, 18. Let start with the first feedback control loop for the 1st diagonal element of $G_{Final}$ as follow:

$$G_{11} = 0.3278 - 0.5170i \tag{6.16}$$

The transfer function considered here is the linear time-invariant system, which is the relationship between virtual input $u_1$ to accelerometer 2. Hence the $T-$matrix representation will be:

$$\bar{T} = \begin{bmatrix} 0.3278 & 0.5170 \\ -0.5170 & 0.3278 \end{bmatrix} \tag{6.17}$$

to which the relative uncertainty associated with the SISO system is

$$rW = \begin{bmatrix} 0.0275 & -0.0722 \\ 0.0722 & 0.0275 \end{bmatrix} \tag{6.18}$$

On the basis of above uncertainty model, a control scenario is considered in order to achieve 90% attenuation of the (unit norm) disturbance requested as nominal performance. As mentioned in Chapter 4, the tuning procedure in the nominal case is the following; that is, LQ controller is easier to be tuned by changing the values of the weight $Q$ and $R$ than $H_\infty$ controller. However, both controllers have been tuned to achieve the same performance level of closed-loop of vibration reduction which is explicitly shown by the weighting function in robust case as

$$W_y(z) = \frac{0.9z - 0.899}{z - 0.9944} \tag{6.19}$$

for which continuous-time equivalent frequency response is depicted in Figure 6.2. In the other hand, no weighting function $W_u(s)$ on the control action has been included in the scheme.

Moreover, the LQ controller does not take model uncertainty into account, which is designed based on the identified model of the system. As contrast, the model uncertainty derived from the identification limitation has been dealt with in design robust HHC controller. Then the design procedure will be conducted with the first transfer function,

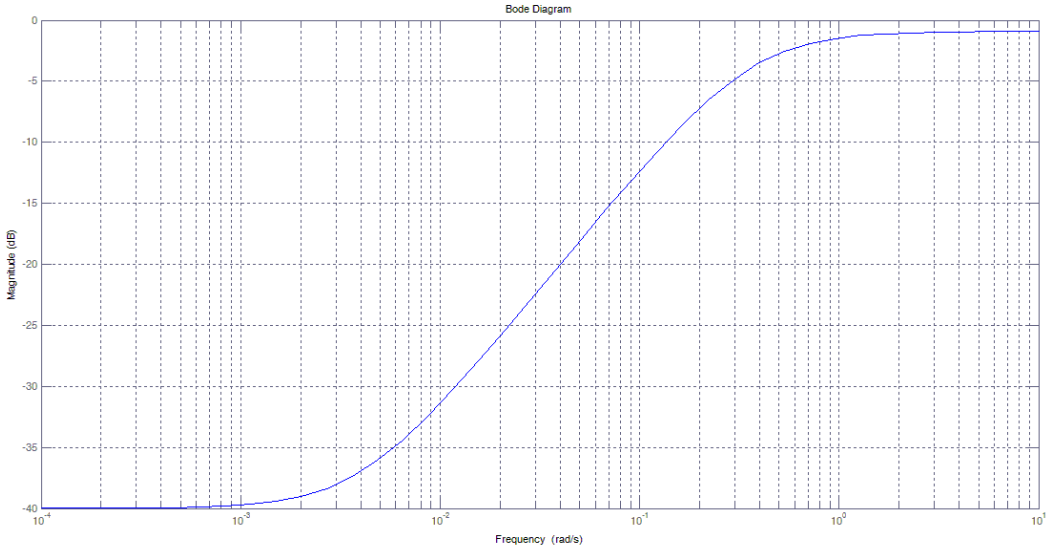


FIGURE 6.2: Frequency response of possible $W_y(s)$ weighting functions.

then repeating for the next three relation between three virtual inputs $u_2$, $u_3$, $u_4$ to accelerometer 9, 10, 18, respectively.

It is obviously recognized that the vibration attenuation level can be easily changed due to the independence of each control loop design. Then two scenarios are considered. The first one aims at keeping the weighting function and both matrices $Q$ and $R$ unchanged for all feedback loops while the second one separates the required performance for each closed-loop steady state attenuation of the vibration. In this thesis, both scenarios are taken into account in order to select the best one.

Hence, to compare the resulting performance of the overall feedback system, a Monte Carlo study was carried out by 500 values chosen randomly for the normalized uncertainty $\Delta$. In the following, the results of this Monte Carlo procedure in terms of steady state attenuation of disturbance are depicted. Figure 6.3 and Figure 6.4 show the control efforts and vibration attenuation performance for overall feedback control loops.

In Figure 6.3, the robust controller inputs are very similar to the LQ controller, which means that the robust controller not only is able to deal with the uncertainty model but also to require less energy to achieve the better performance as compared with LQ controller.

More clearly, in the Figure 6.4, the LQ controller fails to find the correct tradeoff to attain the same level of attenuation for each of measured outputs achieved by the robust HHC controller in this thesis. Moreover, the proposed robust HHC synthesis has another substantial benefit over a classical LQ one; that is, defining weighting functions $W_y$ is

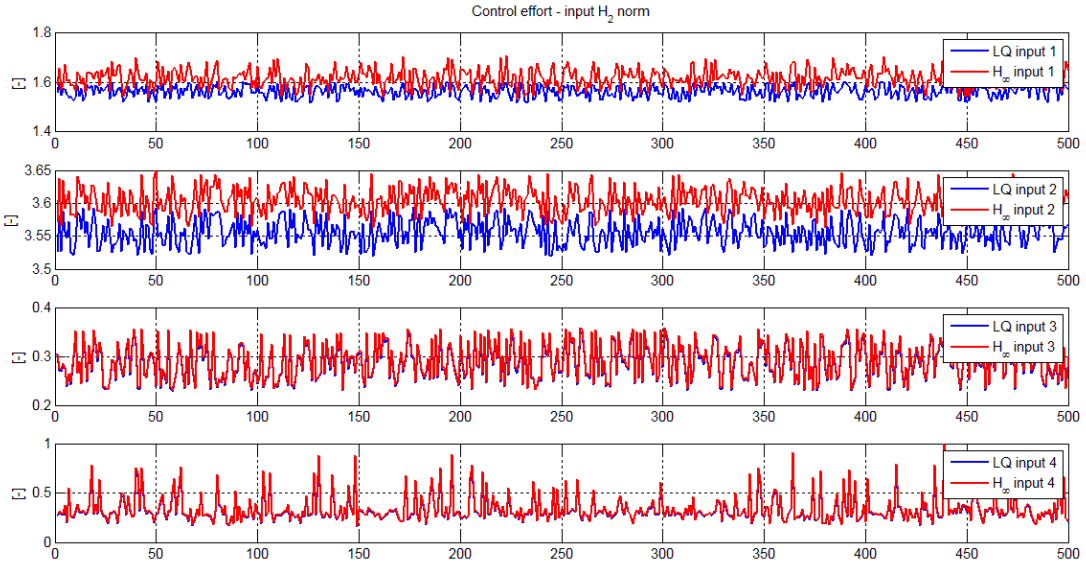


FIGURE 6.3: Control effort of 4 control loops with the same weighting function.

intuitive way which seem to be much more convenient than repeating different $Q$ and $R$ matrices until control required performances have been satisfied. However, it is apparent that the cost of robustness is tradeoff with the settling time. While the robust controller need at least 4 seconds to finish the transient period and reach to the steady state one, a average settling time is shorter in LQ case, which is around 2 seconds.

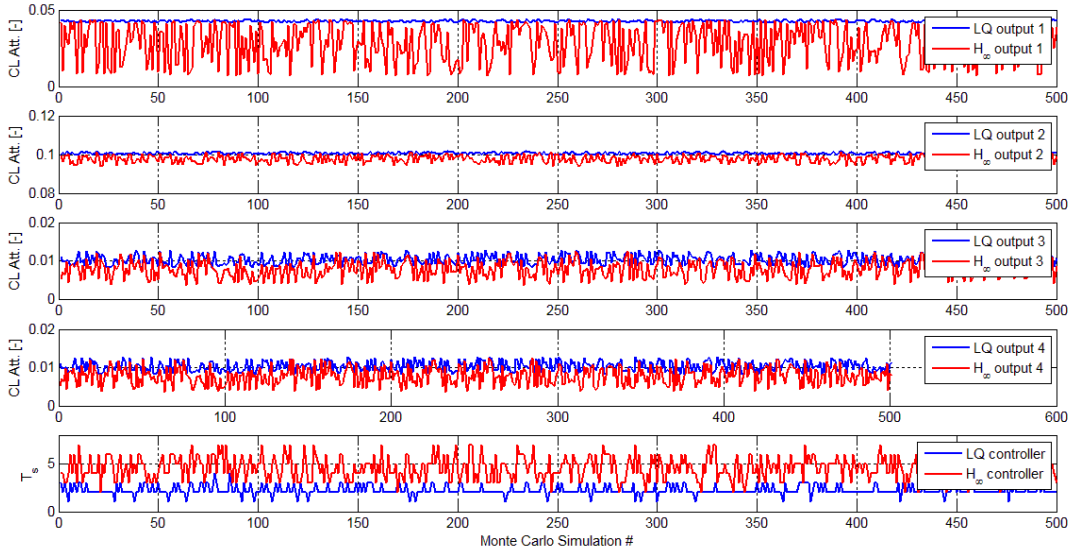


FIGURE 6.4: Closed loop performance comparison between LQ and $H_\infty$ approaches with the same weighting function.

Table 6.3 confirms these advantages and disadvantages of both control synthesis scheme. In all four feedback loop performances, the vibration attenuations of $H_\infty$ approach

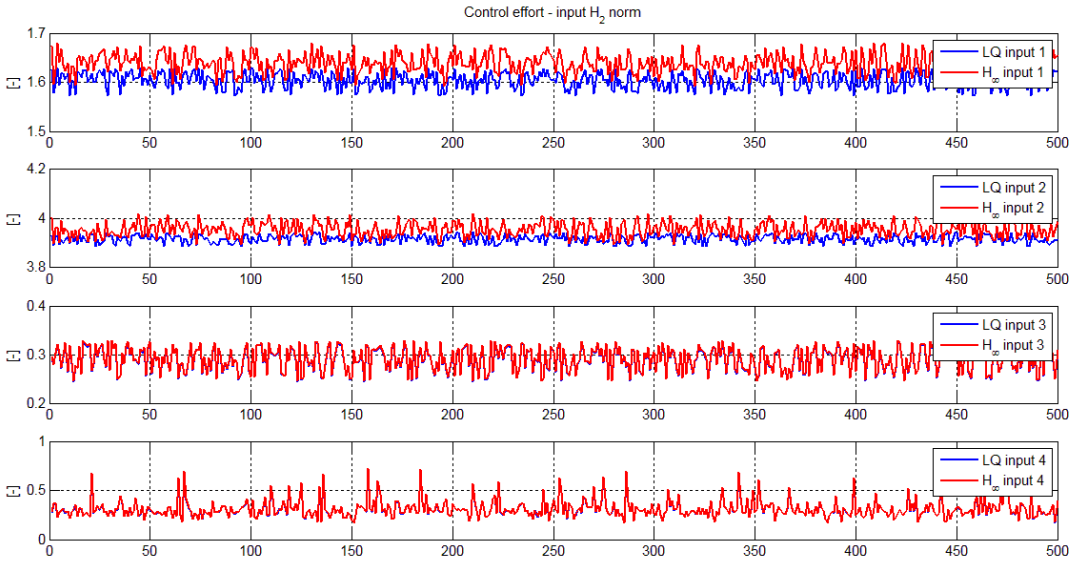


FIGURE 6.5: Control performance of 4 control loops with different weighting functions.

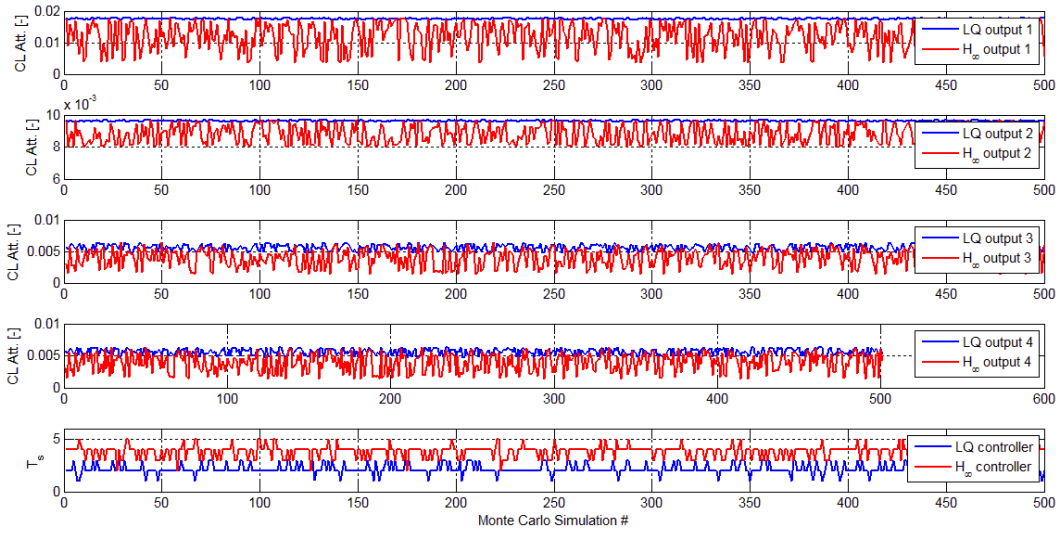


FIGURE 6.6: Closed loop performance comparison between LQ and $H_\infty$ approaches with different weighting function.

are smaller than LQ one. In the first loop, LQ is able to reduce 95% while only 3% vibration's amplitude is measured in accelerometer 2. Moreover, the noise in second LQ feedback loop has been attenuated up to 90%, which is smaller than 8% in the $H_\infty$ case. Finally, both last performances are smaller than 1% for robust controller. Of course, LQ controller always show worse level of noise reduction than robust one.

Moreover, as mentioned, in the synthesis procedure, we have capability in choosing the same noise attenuation performance for all closed-loops or design different weighting functions in term of different transfer function from virtual input to accelerometer. The

| $y_1(LQ)$ | $y_1(H_\infty)$ | Max $y_1(LQ)$ | Max $y_1(H_\infty)$ |
|---|---|---|---|
| 0.042694 | 0.026780 | 0.043809 | 0.043750 |
| $y_2(LQ)$ | $y_2(H_\infty)$ | Max $y_2(LQ)$ | Max $y_2(H_\infty)$ |
| 0.100615 | 0.097548 | 0.101667 | 0.101402 |
| $y_3(LQ)$ | $y_3(H_\infty))$ | Max $y_3(LQ)$ | Max $y_3(H_\infty)$ |
| 0.010327 | 0.007682 | 0.012689 | 0.012625 |
| $y_4(LQ)$ | $y_4(H_\infty))$ | Max $y_4(LQ)$ | Max $y_4(H_\infty)$ |
| 0.010343 | 0.007703 | 0.018209 | 0.018203 |
| $u_1(LQ)$ | $u_1(H_\infty)$ | $u_2(LQ)$ | $u_2(H_\infty)$ |
| 1.563378 | 1.625183 | 3.557116 | 3.605914 |
| $u_3(LQ)$ | $u_3(H_\infty)$ | $u_4(LQ)$ | $u_4(H_\infty)$ |
| 0.286947 | 0.290741 | 0.320387 | 0.331819 |
| $\Sigma(LQ)$ | $\Sigma(H_\infty)$ | $T_s(LQ)$ | $T_s(H_\infty)$ |
| 0.000655 | 0.012666 | 2.238000 | 4.414000 |

TABLE 6.3: Monte Carlo Study: Performance of the controllers based on the LQ and the $H_\infty$ control synthesis with the same noise reduction level.

Figure 6.5 and Figure 6.6 have shown the similar noise reduction level in four measured outputs, which is caused from the fact that it is flexible but time consumption. In detail, the second scenario required four times longer than the first one in sense in adapting the weighting functions.

Based on the above results, the $H_\infty$ approach could be beneficial in term of the reducing the need for adaption in the operation of the HHC system, which would not make only to the easier implementation in the real experimental and true helicopter system but also allow to attain both performance and stability of closed loop behavior.

## 6.5 Conclusion

Although the SVD and RGA are capable to be considered as natural approaches in selection pairing of MIMO system, no application can be applied for this non-square complex transfer function of the vibration system in helicopter. It is very interesting to invent the new idea based on the algebraic properties of RGA in order to design the pre-compensator to transfer previous system to be square-diagonal one. Hence, the two controller LQ and robust HHC are developed based on the compensated model, whose simulation performance are very promising and therefore motivate us to deploy the proposed technique to the real experimental test system as well as helicopter.

# Chapter 7

# Conclusion

In this work, the non-square model of vibration control system in helicopter is introduced, which has been analyzed by Singular Value Decomposition and Relative Gain Array. Two techniques are used not only to find the pairs between inputs and outputs but also to compute the compensator which has transformed the original system to be square-diagonal system. Moreover, we have theoretically shown that the general form of system includes the uncertainty part as well as the nominal part. LQ controller therefore has been designed based on nominal model of the system without considering the uncertainty. In the case of taken the uncertainty into account, the $H_\infty$ controller has shown the better performance in term of the noise attenuation and robustness.

In conclusion, several novelties are presented in this thesis. Firstly, the non-square system has been transformed into the square-diagonal based on the algebraic properties of RGA, which is able to design 4 SISO loop for MIMO system with taking into account the canonical form of uncertainty in original model. Secondly, the LQ and $H_\infty$ controllers are found to gain the vibration attenuation levels and the robustness. Consequently, the weighting functions presented for performance levels have been chosen for each SISO loop or the same for all loops, which would lead to the reduction of tuning effort and is very convenient in service engineers. This property is extremely valuable in industry.

Future work will be developed as following tasks: (i) deploy the algorithm to real helicopter, (ii) develop the algorithm for different non-square model or even the square model with difficulty in choosing the pairs of inputs and outputs, (iii) analysis the theoretical convergence of the algorithm.

(i) The controllers have been found based on the identification model, which can include the big uncertainty due to the complexity of MIMO system. However, the

simulation has illustrated the good performance of both controller in vibration attenuation level and robustness regarding the uncertainty of the process. Therefore, we have capability in deploying the algorithm in the experimental devices or real helicopters.

(ii) The procedure starts from the fact that the transfer function from active actuators to the head phone are changing due to a lot of conditions. This means that in one helicopter, it is able to find several positions of actuator to influence to the noise attenuation in fuselage. The process commonly results to the non-square model, which can be occurred the difficulty in choosing good pairs or impossible. Therefore, the algorithm is expected to work well in several different processes.

(iii) The algorithm is developed based on the function fminsearch in MATLAB, whose idea is to find the minimum of the cost with random small deviation of the initial condition. Consequently, the convergence of the algorithm is questionable.

# Bibliography


[1] S. Skosgestad and I. Postlethwaite. *Multivariable feedback control: analysis and design*. John Wiley & Sons, Ltd, second edition edition, 2005.

[2] G. Mathur J. O'Connell and R. JanakiRam. Helicopter cabin noise reduction using active structural acoustic control. In *The Boeing Company, Marty Johnson, Virginia Tech Dino J. Rossetti, Lord Corporation.*

[3] H. Eisenbeiss. A mini unmanned aerial vehicle (UAV): system overview and image acquisition. *International Archives of Photogrammetry. Remote Sensing and Spatial Information Sciences*, 36(5/W1), 2004.

[4] R. Paradies and P. Ciresa. Active wing design with integrated flight control using piezoelectric macro fiber composites. *Smart Materials and Structures*, 18(3):1–9, 2009.

[5] S. Stupar, A. Simonovic, and M. Jovanovic. Measurement and analysis of vibrations on the helicopter structure in order to detect defects of operating elements. *Scientific Technical Review*, 62(1):58–63, 2012.

[6] R.M. Goodall J.T. Pearson and I. Lyndon. Active control of helicopter vibration. *Computing & Control Engineering Journal*, pages 277–284, December 1994.

[7] M. Lovera, L. Piroddi, F. Boi, and G. L. Ghiringhelli. Black-box mimo model identification for structural vibration reduction in helicopters. In *2015 Advanced Control and Navigation for Autonomous Aeroespace Vehicles Conference, Seville, Spain*, 2015.

[8] W. Corbetta, A. Toso, E. Vigoni, and G.L. Ghiringhelli. Set-up of the A109 mock-up for vibration and acoustic tests, March 2005. FriendCopter Internal Report.

[9] P.P. Friedmann and T. Millott. Vibration reduction in rotorcraft using active control-a comparison of various approaches. *Journal of Guidance, Control and Dynamics*, 18(4):664–673, 1995.

[10] Ch. Kessler. Active rotor control for helicopters: motivation and survey on higher harmonic control. *CEAS Aeronautical Journal*, 1(1-4):3–22, 2011.

[11] Ch. Kessler. Active rotor control for helicopters: individual blade control and swashplateless rotor designs. *CEAS Aeronautical Journal*, 1(1-4):23–54, 2011.

[12] J. Shaw and N. Albion. Active control of the helicopter rotor for vibration reduction. *Journal of the American Helicopter Society*, 26(3):32–39, 1981.

[13] R. Mura, A. M. Ghalamzan Esfahani, and M. Lovera. Robust harmonic control for helicopter vibration attenuation. In *2014 American Control Conference, Portland, USA*, 2014.

[14] R. Mura and M. Lovera. Baseline vibration attenuation in helicopters: robust MIMO-HHC control. In *2014 International Federation of Automatic Control Conference, Cape Town, South Africa*, 2014.

[15] Y. Cao and D. Rossiter. An input pre-screening technique for control structure selection. *Journal of computer and chemical engineering*, 21(6):563–569, 1996.

[16] E.H. Bristol. On a new measure of interations for multivaribale process control. *IEEE Transactions on Automatic Control AC-11*, pages 133–134, 1966.

[17] E.A. Woff. *Studies on Control of Integrated Plants*. PhD thesis, Norwegian University of Science and Technology, Trondheim, 1994.

[18] J. Chandrasekar, Li Liu, D. Patt, P.P. Friedmann, and D.S. Bernstein. Adaptive harmonic steady-state control for disturbance rejection. *IEEE Transactions on Control Systems Technology*, 14(6):993–1007, 2006.

[19] A. M. Zanchettin, A. Calloni, and M. Lovera. Robust magnetic attitude control of satellites. *IEEE/ASME Transactions on Mechatronics*, 18(4):1259–1268, 2013.